Beam Cleaning and Collimation Systems

S. Redaelli
CERN, Geneva, Switzerland

arXiv:1608.03159v1 [physics.acc-ph] 10 Aug 2016

Abstract
Collimation systems in particle accelerators are designed to dispose of unavoidable losses safely and efficiently during beam operation. Different roles are required for different types of accelerator. The present state of the art in beam collimation is exemplified in high-intensity, high-energy superconducting hadron colliders, like the CERN Large Hadron Collider (LHC), where stored beam energies reach levels up to several orders of magnitude higher than the tiny energies required to quench cold magnets. Collimation systems are essential systems for the daily operation of these modern machines. In this document, the design of a multistage collimation system is reviewed, taking the LHC as an example case study. In this case, unprecedented cleaning performance has been achieved, together with a system complexity comparable to no other accelerator. Aspects related to collimator design and operational challenges of large collimation systems are also addressed.

Keywords
Beam collimation; multi-stage cleaning; beam losses; circular colliders; Large Hadron Collider.

1 Introduction

The role of beam collimation systems in modern particle accelerators has become increasingly important in the quest for higher beam energies and intensities. For reference, the beam stored energy of recent and future particle accelerators is shown in Fig. 1, which includes the design (362 MJ) and achieved (150 MJ) values of the CERN Large Hadron Collider (LHC) [1], as well as the 700 MJ goal for its high-luminosity upgrade (HL-LHC) [2, 3]. High-power accelerators simply cannot operate without adequate systems to control unavoidable losses in standard beam operation. The operation and physics goals of recent superconducting, high-energy hadron colliders, such as the Tevatron [4], the Relativistic Heavy-Ion Collider [5], and the LHC, could not be fulfilled without adequate beam collimation. With the LHC, the design complexity and the performance of beam collimation has achieved unprecedented levels. This is required to 'clean' beam losses efficiently before they reach the small apertures of superconducting magnets. As illustrated in Fig. 2, the inner aperture of LHC magnets sits only a few centimetres apart from the circulating beams, which carry a total energy more than a billion times larger than that necessary to perturb the operation of superconductors.

In this document, the design of collimation systems for hadron accelerators is presented, with a special focus on the requirements and design aspects of high-energy and high-intensity machines. The general scope of a collimation system is to dispose, safely and in a controlled way, of beam losses that would otherwise occur at sensitive locations or on accelerator equipment that is not designed to withstand beam losses. In practice, this general definition finds its concrete implementations depending on the specific design goals required for a given accelerator. For example, collimation requirements are different for 'warm' high-power machines, where loss localization is crucial, than for 'superconducting' accelerators, where operation efficiency is ensured by keeping losses in cold magnets below quench limits. The roles of collimation systems in accelerators are discussed in Section 2. In Section 3, some basic notation is introduced and the inputs to collimation design from machine aperture and beam loss mechanisms are discussed. The design of a multistage collimation system is outlined in Section 4.

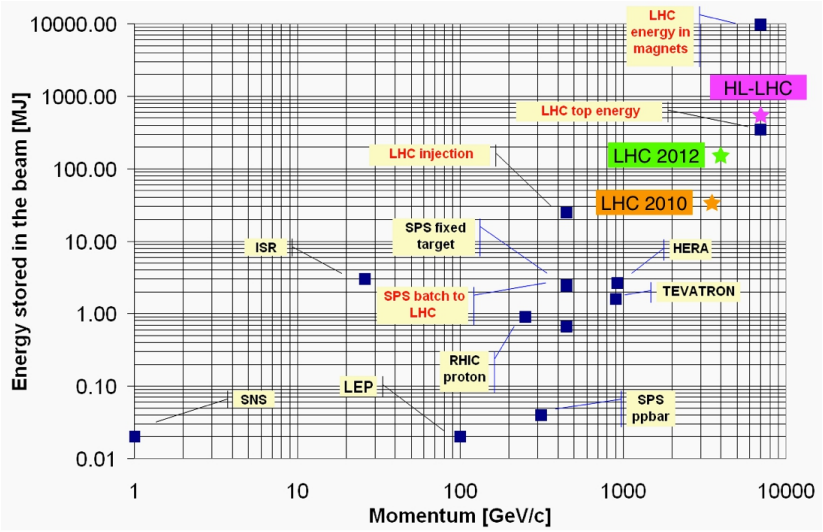

Fig. 1: Livingston-like plot of beam stored energy achieved and planned for different present and future particle accelerators. Courtesy of J. Wenninger.

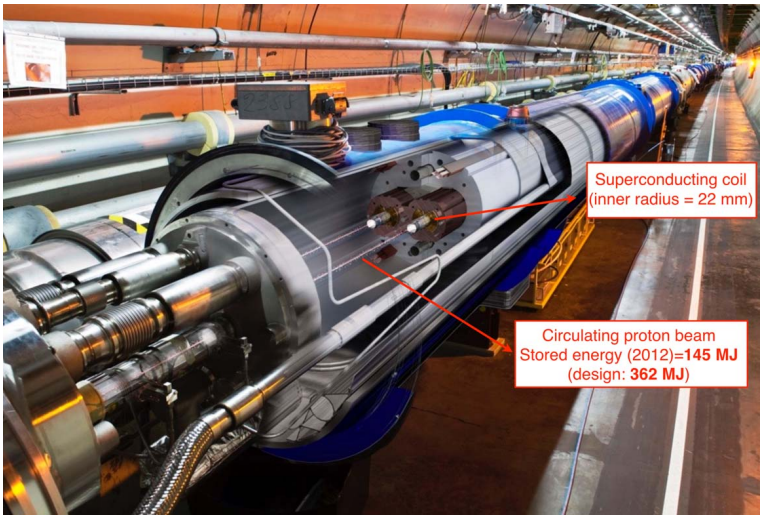

Fig. 2: The LHC dipole in the tunnel, showing the cross-section of the magnet cold mass. The inner horizontal and vertical half dimensions of the dipole beam screen are 22 mm and 17 mm, respectively.

The second part of this document is focused on the presentation of the LHC collimation system as a case study. In Section 5, the system layout is reviewed and operational challenges for beam collimation are introduced, presenting the solutions deployed at the LHC. The LHC collimator design is discussed in Section 6 and the collimation performance achieved in LHC run I [6], at energies of up to 4 TeV and stored beam energies of 150 MJ, is reviewed in Section 7. The lecture is concluded with a brief review of advanced collimation concepts that are being considered for upgrading the present LHC collimation and for implementation in future accelerators under study. This is presented in Section 8.

2 Roles of collimation systems in particle accelerators

Typical roles of collimation systems are summarized in the following.

– **Cleaning of betatron and off-momentum beam halos**: Unavoidable beam losses of halo particles must be intercepted and safely disposed of before they reach sensitive equipment. The required cleaning performance depends on the design of the accelerator. The most challenging

requirements arise for superconducting accelerators, where loads from beam losses must remain below the quench limits of superconducting magnets. For example, the LHC design beam stored energy of 362 MJ has to be compared with typical quench limits of a few tens of mW/cm^3 [7].

- **Passive machine protection**: Collimators are the closest elements to the circulating beam and represent the first line of defence in various normal and abnormal loss cases, as discussed in several companion lectures at this school. Owing to the damage potential of hadron beams, this functionality has become one of the most critical aspects of the operation of accelerators [8, 9], as well as a crucial input to the design of collimators that must withstand design failures.
- **Cleaning of collision products**: In colliders, this is achieved with dedicated movable collimators located in the outgoing beam paths of each high-luminosity experiment, to catch the products of collisions: direct collision debris and beam particles that emerge from the collision points with modified angles and energy.
- **Optimization of the experiment background** (i.e., minimization of halo-induced noise in detector measurements): this is one of the classical roles of collimation systems in previous colliders. Beam tail scraping or local shielding at the detector locations can reduce spurious signals in detectors (see, for example, a recent report [10]).
- **Concentration of radiation doses**: for high-power machines, it is becoming increasingly important to be able to localize beam losses in confined and optimized 'hot' areas rather than having a distribution of many activated areas along the machine. This is an essential design requirement for collimation systems, to allow easy access for maintenance in the largest fraction of the machine.
- **Local protection of equipment for improved lifetime against radiation effects**: Dedicated movable or fixed collimators are used to shield equipment locally. For example, passive absorbers are used in the LHC collimation inserts to reduce total doses, and to warm dipoles and quadrupoles that would otherwise have a short lifetime in the high-radiation environment foreseen during the nominal LHC operation. The exposure of radiation to equipment might not pose immediate limitations to operation of a machine but its optimization is crucial to ensure long-term reliability.
- **Beam halo scraping and halo diagnostics**: Though rarely a driving design criterion, the possibility to scan the beam distribution actively can be a very useful functionality of a collimation system. Collimator scanning in association with sensitive beam loss monitoring systems proved a powerful method of probing the population of beam tails [11, 12], which are otherwise too small, compared with the beam core, to be measured by conventional emittance measurements. Thanks to their robustness, the LHC primary collimators can be efficiently used to scrape and shape the beams, as in Ref. [13]. Full beam scraping also provides precise, though destructive, measurements of beam sizes.

A collimation system might typically fulfil several roles. For example, the concentration of radiation losses or the reduction of experimental background are natural by-products of a very efficient beam collimation design. Conversely, before designing a collimation system, it is important to identify the driving requirements for its design in a specific accelerator. For the LHC, the driving design criterion is halo cleaning, which must be excellent to operate the machine below the quench limit of the superconducting magnets at maximum beam energy. It is interesting to note that the present LHC beam collimation [1, 14] is quite special in that it fulfils all the roles listed, thanks to a careful design that has been extended beyond the cleaning functionality. The price to pay for this performance is the unprecedented complexity, which poses important operational challenges, as discussed in Section 7.

3 Inputs to collimation design from aperture and beam loss mechanisms

3.1 Basic definitions for collimation and beam halo

Particles with transverse amplitudes or energy deviations significantly larger than those of the reference particle are referred to as *beam halo particles*. One can distinguish between *betatron* and *off-momentum*

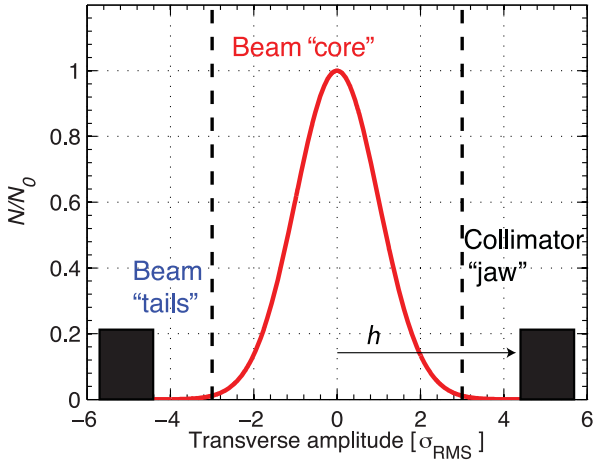

Fig. 3: Gaussian distribution, which is typically adequate to model the particle distribution of the beam core (red line). Overpopulated tails may be intercepted by collimator jaws, which constrain particle motion at a given transverse betatron amplitude.

halos, which are formed in the case of larger-than-nominal transverse emittance or energy error, respectively. The transverse amplitude of a particle i around a closed orbit, $z \equiv (x, y)$, can be expressed as a function of the longitudinal curvilinear coordinate s for the Twiss parameters $\beta_z(s)$, $D_z(s)$, and $\phi_z(s)$ as

$$z_i(s) = \sqrt{\beta_z(s)\epsilon_{z,i}}\sin[\phi_z(s) + \phi_{z,i,0}] + \left(\frac{\delta p}{p}\right)_i D_z(s) \,, \tag{1}$$

where $\epsilon_{z,i}$ is the single-particle emittance, $(\delta p/p)_i$ is the energy error, and $\phi_{z,i,0}$ is an arbitrary phase. The r.m.s. size of the beam at location s is then given by

$$\sqrt{\beta_z(s)\epsilon_z + \left(\frac{\delta p}{p}\right)^2 D_z^2(s)} \,, \tag{2}$$

where ϵ_z and $\delta p/p$ are the r.m.s. transverse emittance and energy spread of the beam. The notation to express the machine aperture and the collimator settings will use, unless specified otherwise, the *betatron beam size*,

$$\sigma_z(s) = \sqrt{\beta_z(s)\epsilon_z} \,, \tag{3}$$

which takes into account only the contribution to the beam size from the betatron motion. Collimator settings might then be given in normalized units as

$$n_\sigma = \frac{h}{\sigma_z} \,, \tag{4}$$

where h is the distance in millimetres between the collimator jaw and the circulating beam (e.g., the half gap of a two-sided collimator centred around the beam, as shown in Fig. 3).

The distinction between halo and core particles is, to a certain extent, arbitrary. For Gaussian distributions, one may define as halo particles those with amplitudes above three r.m.s. deviations of the Gaussian (see dashed lines in Fig. 3), i.e., with emittances larger than $9\epsilon_z$. For a beam with perfect two-dimensional Gaussian distributions in the (z, z') plane, about 1.1% of the total beam particles have amplitudes above $3\sigma_z$ and 0.03% above $4\sigma_z$, respectively. Particles this far out from the beam core are rarely of any use for accelerators and are more likely to cause nuisances (beam losses, irradiation of components, background in detectors, etc.). For off-momentum halos, a similar definition could be adopted. For other purposes in circular accelerators, one might consider as halo the particles outside the

RF bucket that are lost when beams are accelerated or in the presence of synchrotron radiation (which is non-negligible at the LHC).

Beam collimation is achieved by placing blocks of material, the *collimator jaws*, close to the circulating beams, to constrain the betatron amplitudes of stray particles outside the core. This is shown schematically by the black boxes in Fig. 3. Collimation of off-momentum tails might be achieved in a similar way as for betatron tails, by placing collimators at locations of high dispersion, where the particle's energy shift results in a transverse offset, as in the second term on the right-hand side of Eq. (1).

How close to the beam a collimator should be depends on various aspects that will be elaborated on in the rest of this paper. In particular, it will be shown that the outer limit for a collimator setting depends on the available machine aperture that needs to be protected and on the cleaning performance that needs to be achieved. The inner limit depends essentially on how collimators perturb beam stability through an increase in the machine impedance. Tighter settings also typically lead to higher beam losses and tighter positioning tolerances against orbit movements and optics errors. Thus, collimators should not be set closer to the beams than is strictly necessary.

3.2 Collimation cleaning inefficiency

The cleaning performance of a collimation system is measured by the *collimation efficiency*, a figure of merit that expresses the fraction of halo particles 'caught' by the system over the total lost from the beam. A perfect beam collimation provides 100% cleaning, i.e., there is no beam loss at sensitive equipment. Alternatively, the *cleaning inefficiency*, η_{c}, can be introduced as the relative fraction of beam that 'leaks' to other accelerator components, A_{lost}, compared with what is intercepted and safely disposed of by the collimators, A_{coll}:

$$\eta_{\mathrm{c}} = \frac{A_{\mathrm{lost}}}{A_{\mathrm{coll}}} \,. \tag{5}$$

The relevant measure of 'beam loss', indicated as A in this equation, has to be identified for the specific design criteria that the collimation system addresses.

The LHC beam collimation requirements are driven by the challenge to keep beam losses below the quench limits of the superconducting magnets. In this case, the inefficiency η_{c} is defined as the number of protons lost as a fraction of the total number of particles absorbed by the collimation system. The *local cleaning inefficiency*, $\tilde{\eta}_{\mathrm{c}} \equiv \tilde{\eta}_{\mathrm{c}}(s)$, is defined as a function of the longitudinal coordinate s as the fractional loss per unit length,

$$\tilde{\eta}_{\mathrm{c}} = \frac{\eta_{\mathrm{c}}}{L_{\mathrm{dil}}} = \frac{N(s \to s + \Delta s)}{N_{\mathrm{abs}}} \frac{1}{\Delta s} \,, \tag{6}$$

where $N(s \to s + \Delta s)$ is the number of particles lost over the distance Δs, i.e., in the longitudinal range $(s, s + \Delta s)$, and N_{abs} is the number of particles absorbed by the collimation system.

This definition has the advantage that it can be directly compared with the quench limits of superconducting magnets if a proper *dilution length* is chosen. Indeed, for the LHC it was estimated [15] that the quench limits in units of proton lost per unit length, R_{q}, are

$$R_{\mathrm{q}}^{\mathrm{inj}} = 7.0 \times 10^{8} \text{ protons}/(\mathrm{m} \cdot \mathrm{s}) \ (450 \text{ GeV}) \,, \tag{7}$$

$$R_{\mathrm{q}}^{\mathrm{top}} = 7.6 \times 10^{6} \text{ protons}/(\mathrm{m} \cdot \mathrm{s}) \ (7 \text{ TeV}) \,, \tag{8}$$

for beams at injection (inj) and top (top) energies, respectively. These approximate figures were used early in the LHC design phase and in first collimation performance estimates [16]. Although nowadays detailed simulation tools and more adequate models are available to compare peaks of energy deposition in the magnet coils directly against quench limits of superconducting cables (see, for example, Ref. [7]), the formalism introduced here is very useful to introduce challenges for collimation design, as discussed next.

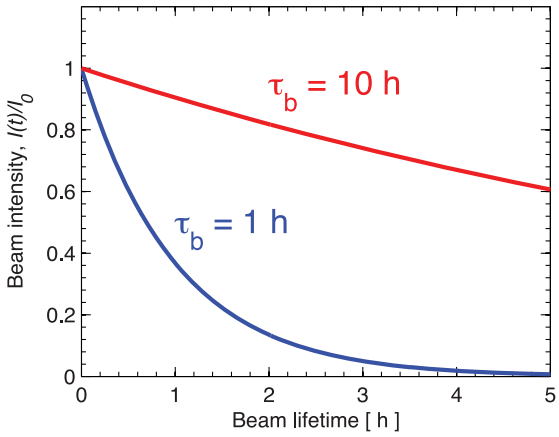

Fig. 4: Relative reduction of beam current versus time, $I(t)/I_0$, for beam lifetime values of 1 h and 10 h

3.3 Beam lifetime and loss modelling

There are various mechanisms that lead to losses in particle accelerators, as also discussed in companion lectures at this school [8, 9]. One can distinguish between *regular* and *abnormal beam losses*, referring to unavoidable losses that occur during standard operation, as opposed to losses caused by failures of accelerator systems or by wrong beam manipulations. For both categories, losses might occur over a broad range of time-scales, from a fraction of a single turn to tens of seconds.

In circular colliders, a main source of loss comes from the collisions of the opposing beams that cause burn-off of beam particles. Other sources of loss are interactions with residual gas, intrabeam scattering, beam instabilities of various types (single-bunch, collective, beam–beam, etc.), the noise of feedback systems used to stabilize beams, transverse and longitudinal resonances, include RF noise. Other losses inherent to operation phases of the accelerator, such as capture losses at the beginning of the ramp, injection and dump losses, losses during dynamics changes of the operational cycle (orbit drifts, optics changes, energy ramp, etc.), are referred to as 'operational losses' [17].

Ignoring, for the moment, very fast loss scenarios and their impact on collimator design [8, 9], let us consider the requirements for beam collimation in the presence of *diffusive losses*. In this case, the transverse increase of particle action per turn is much smaller than one sigma of the r.m.s. distribution. Rather than treating each loss mechanism in detail, losses are modelled by considering the beam lifetime.

The time-dependent circulating beam intensity, $I(t)$, can, for most practical purposes, be modelled by an exponential decay function whose time constant, $\tau_\mathrm{b} \equiv \tau_\mathrm{b}(t)$, defines the *beam lifetime* as

$$I(t) = I_0 \mathrm{e}^{-t/\tau_\mathrm{b}}, \tag{9}$$

for an initial beam current I_0. After a time τ_b, the total beam current is reduced to about 37%. Example profiles of relative beam intensity versus time, $I(t)/I_0$, are shown in Fig. 4 for lifetime values of 1 h and 10 h. In a linear approximation, beam loss rates, $\mathrm{d}I/\mathrm{d}t$, are inversely proportional to τ_b and can be calculated as

$$-\frac{1}{I}\frac{\mathrm{d}I}{\mathrm{d}t} = \frac{1}{\tau_\mathrm{b}}\,. \tag{10}$$

It is important to emphasize that $\tau_\mathrm{b}(t)$ is indeed a function of time and is not constant through the operational cycle. The sources of beam losses introduced previously—operational losses and other accelerator physics mechanisms—occur at different times and might become apparent as drops of beam lifetime at given times in the cycle. An example of measured τ_b during LHC fills for physics is shown in Fig. 5. In 2012, proton beams were accelerated to 4 TeV, whereas in 2011 the maximum energy was 3.5 TeV. The machine configuration and TCP settings were different in these runs.

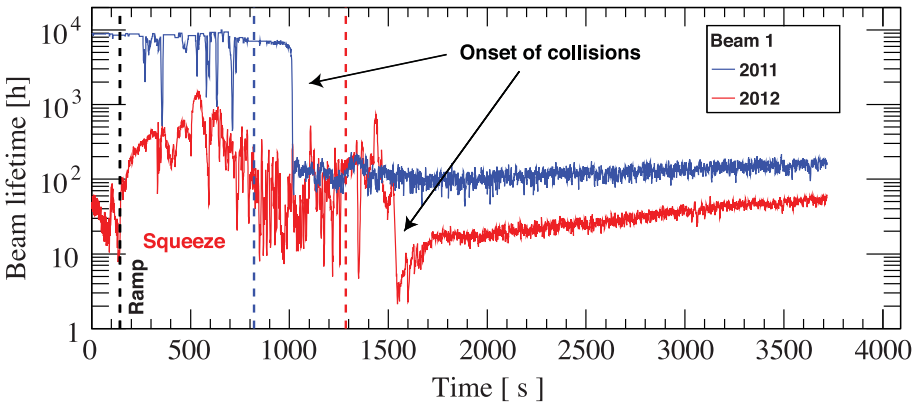

Fig. 5: Measured beam lifetime LHC during two typical LHC physics fills in 2011 at 3.5 TeV (blue) and in 2012 to 4 TeV (red), as a function of time in the cycle. The ramp and squeeze durations were different, so the onset of collisions (reduction in τ_b indicated by black arrows) started at different times. The primary halo cut in the betatron cleaning insertion changed from $5.7\sigma_z$ to $4.3\sigma_z$ for $\epsilon_z = 3.5$ µm. Courtesy of B. Salvachua.

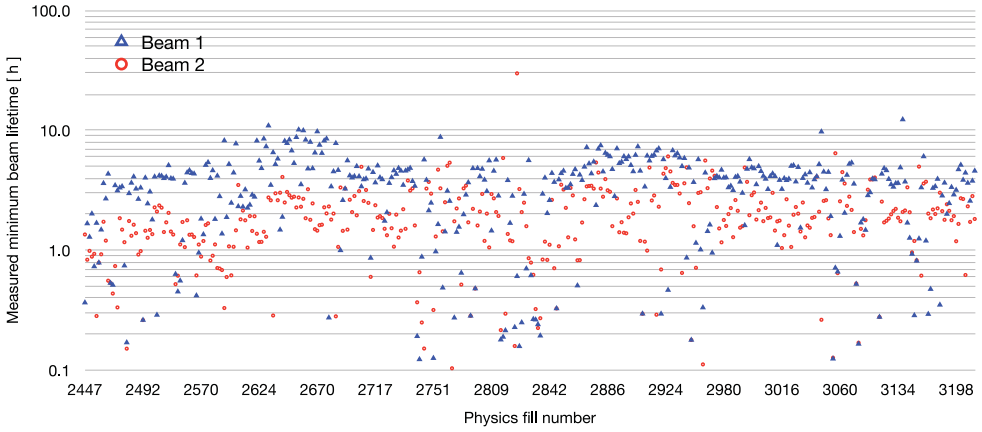

Fig. 6: Minimum lifetime measured during the squeeze of physics fills in 2012 as a function of fill number (to be considered as arbitrary unit). Courtesy of B. Salvachua.

A collimation system must be designed to cope with the maximum expected rates of beam loss. This is determined by the *minimum allowed beam lifetime*, $\tau_b^{\min}$, throughout the operational cycle, most notably during phases at maximum energy (flat-top, squeeze, collision preparation, and physics data recording) when the beam stored energy is largest. The design value used to specify the LHC collimation system is $\tau_b^{\min} = 0.2$ h for up to a maximum time of 10 s [15]. The minimum lifetime measured during the squeeze process in 2012 is shown in Fig. 6. Values of τ_b below 1 h were recorded on a regular basis, with several cases even below 0.2 h. The same behaviour at higher beam intensity and energy, as expected in 2015, will cause frequent beam dumps, with a severe impact on LHC operation.

4 Design of a multistage collimation system

4.1 Design requirements and work flow

The LHC case of beam collimation in the presence of high-energy and high-intensity proton beams is considered here. For the collimation system to fulfil the required cleaning goals, it must be ensured that:

(1) the aperture bottlenecks of the accelerators are geometrically shielded such that, for all loss scenarios, primary beam losses hit first collimators;

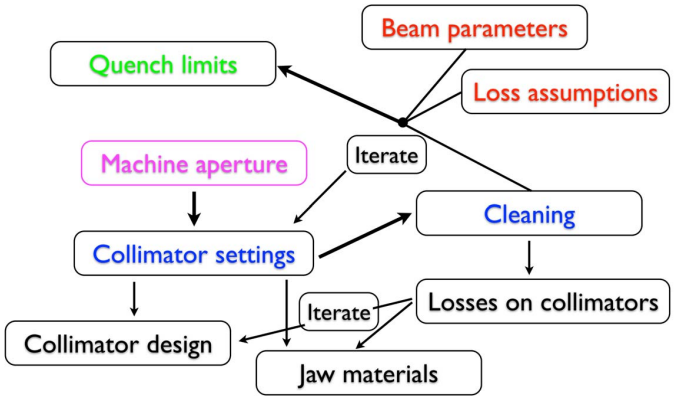

Fig. 7: The various ingredients and competencies required to design a complete collimation system

(2) the total energy carried by the beam, i.e., out-scattered beam particles and the secondary products of beam particles' interactions with the collimator matter, is absorbed within the collimation region, with tolerable leakage to sensitive equipment, notably to cold magnets, for any relevant loss scenarios;

(3) the collimators themselves and other equipment installed in the collimation regions must withstand, without damage, beam losses for different design scenarios;

(4) the contribution to machine impedance from the collimator materials approached to the beam must be tolerable and ensure that the high-intensity beams remain stable.

This last aspect is particularly critical when it comes to designing collimators and absorbers. For more details, see a companion lecture [18]. The complete design of a complex system like that of the LHC requires several steps and iterations between different domains that go well beyond the field of accelerator physics. Figure 7 shows relevant steps towards a complete design of a collimation system. As indicated, several iterations are required.

The understanding of the machine aperture and the required cleaning determines a specification of the collimator settings that can be used to calculate the collimation cleaning. With the input of loss assumption and machine parameters, the first cleaning estimates are compared with the quench limits. This initial design phase is worked out in this section. Closing this loop provides a first conceptual design, which is then used for detailed collimator design. Cleaning simulations also provide distributions of losses on the collimators that are used, in an iterative process, to specify adequate collimator design and jaw material choices. This aspect will not be discussed in this document (see Ref. [18] for more detail).

4.2 Beam cleaning specifications

The total design beam intensity of the LHC beams is $I_{\rm tot} = 2808 \times 1.15 \times 10^{11}$ protons, i.e., 3.2×10^{11} protons, where $n_{\rm b} = 2808$ is the number of bunches and $I_{\rm b} = 1.15 \times 10^{11}$ protons is the bunch population. At the minimum allowed lifetime of 0.2 h, this corresponds to a proton loss rate of 4.4×10^{11} protons/s. At 7 TeV, the beam stored energy is 362 MJ and loss rates approach 500 kW. By expressing the quench limits in the approximate formulation of Eq. (8), one can derive a specification for the local cleaning inefficiency in a cold magnet as

$$\tilde{\eta}_{\rm c} \leq \frac{1}{10000}[1/{\rm m}] \, . \tag{11}$$

Although simulation tools are now available to combine particle tracking and energy deposition simulations, so as to evaluate precisely the energy lost in the superconducting magnet coils, it is very useful to

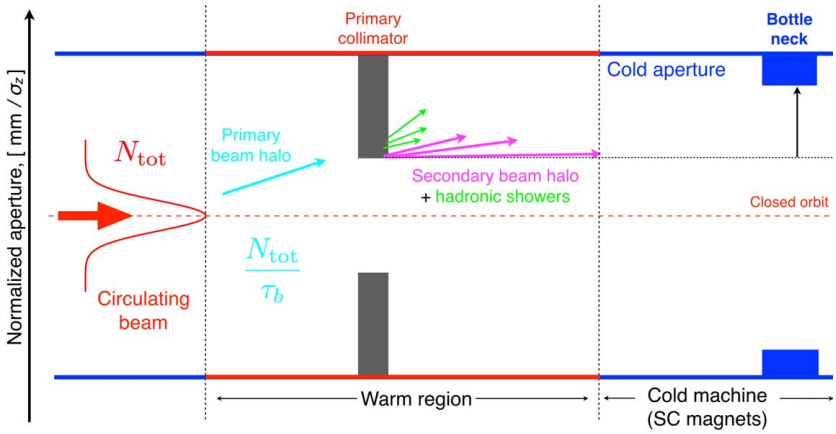

Fig. 8: Single-stage collimation system: SC, superconducting

follow this approximate approach. This formalism provides a powerful tool for designing a collimation system. The number of protons lost per unit length can be simulated with a fast and accurate set-up [19], which provides an essential design optimization tool. Final validation of collimation solutions then follows, using more sophisticated tools that also involve energy deposition simulations [20].

4.3 Machine aperture and collimator settings

To design a betatron cleaning system, one must first compute the available aperture of the accelerator. Let us assume that the circulating beam sees an isolated *aperture bottleneck*, $A_{\mathrm{min},z}$, in the transverse plane z. This is defined as the smallest normalized transverse aperture at any location around the ring. For convenience, the aperture is normalized by the local betatron beam size σ_z. The limiting location is calculated as

$$\hat{A}_{\mathrm{min},z} = \min\left[\frac{A_z(s)}{\sigma_z(s)}\right] , \tag{12}$$

where the minimum is calculated for all locations s around the ring and $A_z(s)$ is the distance in millimetres between the circulating beam and the mechanical aperture. This quantity can be measured directly in an accelerator [21, 22]. While, operationally, it is convenient to express $A_{\mathrm{min},z}$ for a given beam emittance, what matters is actually the *aperture acceptance* $A_z(s)/\sqrt{\beta_z}$. A cold aperture bottleneck is indicated in Fig. 8 as a blue box, and projects into the nominal aperture.

The minimum aperture calculated during the LHC design phase [16] for both planes and beams at injection and top energy are listed in Table 1. Calculations relied on a conservative approach [23] that ensured adequate margins during beam commissioning. While measurements during LHC run I [24] indicated that the LHC aperture is indeed larger than assumed, such conservative figures are considered in this lecture for the collimation design.

4.4 Single-stage collimation

Designing a collimation system involves finding an optics solution and an arrangement of collimators that ensure that losses in cold magnets remain below the quench limits for all design loss rates. In an ideal machine without beam losses, there would be no need for beam collimation, if the minimum machine aperture were at a safe distance from the beam core. In practice, various beam loss mechanisms cause outwards drifts of halo particles, which eventually hit the aperture if there is no mechanism to intercept them. The deposited energy at this location would then depend on the primary beam loss rates, $N_{\mathrm{tot}}/\tau_{\mathrm{b}}$.

One could build a simple single-stage collimation system by placing a primary collimator (TCP; 'target collimator, primary') that intercepts beam losses. Preferably, collimators are placed in a warm region, as far as possible from superconducting magnets. The collimator jaws must be set at a transverse

Table 1: Minimum horizontal and vertical apertures at injection (450 GeV) and top energy (7 TeV, $\beta^* = 0.55$ m) for warm and cold elements, as estimated in the LHC design phase [16].

	450 GeV		**7 TeV**	
	Warm	**Cold**	**Warm**	**Cold**
Beam 1				
Horizontal	6.8	7.9	28	8.9
Vertical	7.7	7.8	8.3	8.4
Beam 2				
Horizontal	6.7	7.7	28	8.1
Vertical	7.7	7.6	8.7	8.8

aperture below that of the machine bottleneck, $\hat{A}_{\mathrm{TCP}} \leq \hat{A}_{\mathrm{min},z}$. This simple system would work if the TCP were a black absorber that could stop all the primary particles at their first passage through the jaw. Also note that, because of the mixing of positive and negative amplitudes of halo particles from the betatron motion, a single-jaw collimator suffices to protect the aperture against slow diffusive losses. (For standard losses, impact parameters in the submicrometre range are expected [25]. At this scale, particles do not see the full jaw length at their first passage because of jaw flatness and surface roughness errors. This increases the inefficiency of a single-stage cleaning system, as more turns are required before particles accumulate enough interactions with the TCP.)

The single-stage system of Fig. 8 does not provide sufficiently efficient halo cleaning. The halo protons that are out-scattered before being absorbed by the jaw material leave the collimator at larger normalized amplitudes and modified energies. These particles populate the so-called *secondary beam halo*, which risks being lost in the machine before interacting again with the collimator in subsequent turns. In addition, the products of hadronic and electromagnetic showers are not contained in the collimator volume and might reach sensitive elements without additional downstream collimators or absorbers.

The cleaning performance of the single-stage system described here was simulated under the assumption that a horizontal TCP is installed in the current LHC betatron cleaning insert. The tools in Ref. [19] allow one to calculate the number of halo protons lost in the collimators and machine aperture. Simulations properly model the proton tracking through the magnetic elements and the scattering in the collimator materials. In Figs. 9 and 10, the predicted local cleaning inefficiency of Eq. (6) is given as a function of the longitudinal coordinate s.

In these cleaning inefficiency plots, black peaks indicate losses at collimators (only one TCP in this case), blue peaks indicate losses at cold magnets and red peaks indicate losses at warm elements. It can be seen, by looking at Fig. 10, which shows zoomed plots around various interaction points, that cold losses reach cleaning inefficiency levels of up to $0.01\,/\mathrm{m}$. This estimate, which is made for a perfect machine without errors, and which does not take into account the energy deposited by hadronic showers, indicates losses at least two orders of magnitude higher than the value specified in Eq. (11). One can therefore conclude that a single-stage collimation system is inadequate for high-intensity superconducting machines, such as the LHC.

4.5 Multistage collimation

The performance of a single-stage cleaning system can be improved with additional collimators downstream of the TCP to catch the secondary halo particles, as shown in Fig. 11. These are called secondary collimators (target collimators, secondary; TCSs) and are typically longer than TCPs, to maximize the absorption of particles out-scattered at the TCPs. On the one hand, the TCS aperture must be larger

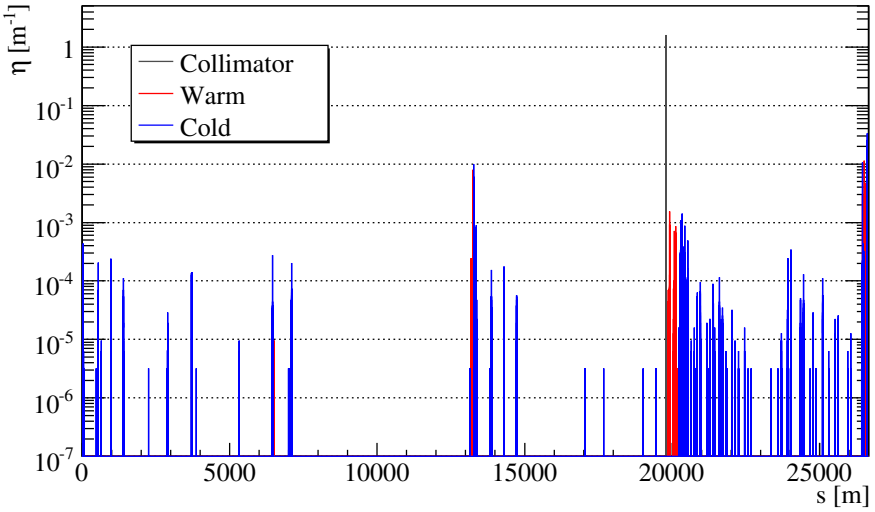

Fig. 9: Simulated cleaning inefficiency at the LHC for a single-stage collimation system achieved with one horizontal primary collimator (TCP) located at the beginning of the LHC warm betatron cleaning insert. The position of the existing primary collimators, i.e., $s = 19.8$ km, is used. Courtesy of D. Mirarchi.

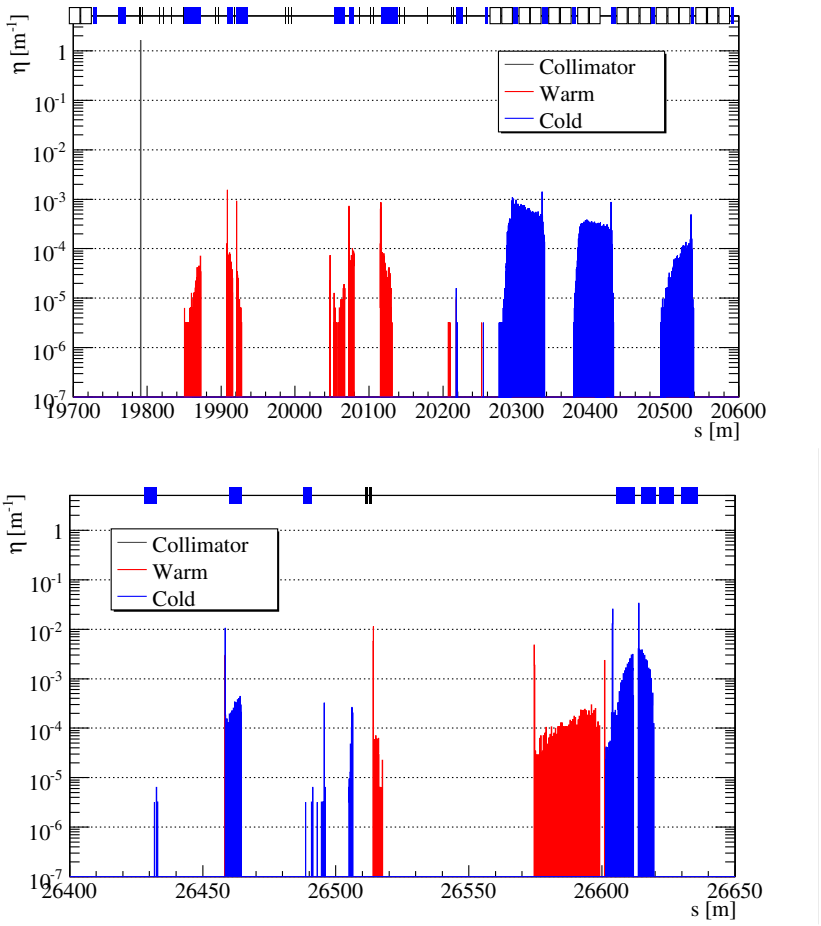

Fig. 10: Enlargement of Fig. 9 in the regions immediately downstream of the cleaning insertion (top) and upstream of the ATLAS experiment (bottom). Courtesy of D. Mirarchi.

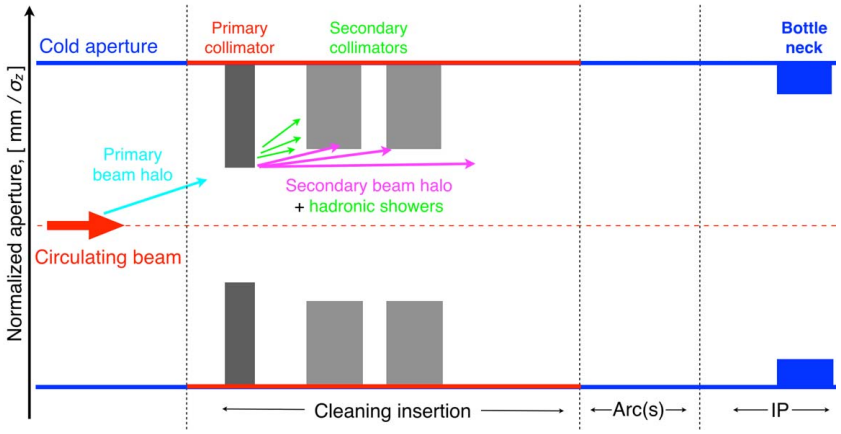

Fig. 11: Two-stage beam collimation system, obtained by adding a set of secondary (TCS) collimators to the single-stage cleaning system of Fig. 8. IP, interaction point.

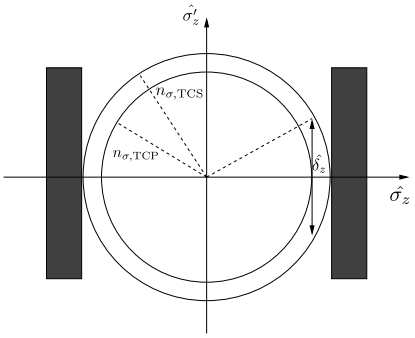

Fig. 12: Normalized phase space with the circumferences radii $n_{\sigma,\mathrm{TCP}}$ and $n_{\sigma,\mathrm{TCS}}$. A normalized kick $\hat{\delta}'$, as in Eq. (13), is necessary for halo particles impinging on the TCP to reach the TCS aperture.

than that of the TCP, to ensure that the *collimation hierarchy* is respected without the risk of a TCS becoming closer to the beam than the TCP, which would result in a single-stage system similar to the one discussed earlier. On the other hand, the TCS aperture should be small enough to maximize its efficiency in catching the particles out-scattered by the TCPs. From Fig. 12, one can calculate the kick of particles impinging on the TCP necessary to reach the amplitude of the TCS as

$$\hat{\delta}' = \frac{\delta'}{\sigma'} = \sqrt{n^2_{\sigma,\mathrm{TCS}} - n^2_{\sigma,\mathrm{TCP}}}\,, \tag{13}$$

where $\sigma' = \sqrt{\epsilon/\beta}$ is the r.m.s. divergence. Such a kick is typically accumulated after multiple passages through the TCP. For a given TCS–TCP retraction, the longitudinal positions of the TCS collimators must be optimized to intercept secondary halo particles. This is illustrated in Fig. 13 for a one-dimensional case. This condition is respected at betatron phase advances, where the multiple Coulomb scattering angle translates into maximum offsets in the collimation plane.

The problem of optimum phase locations for a two-stage collimation system is worked out in detail in Ref. [26]. Finding a solution is more complicated than appears in Fig. 13 because scattering occurs in all directions. A one-dimensional model is thus not adequate. However, it can be demonstrated that an arrangement of primary and secondary collimators in three planes (horizontal, vertical and skew) can be found to ensure satisfactory multiturn cleaning [26].

Detailed performance analysis of a two-stage cleaning process for the LHC was conducted in the design phase [16]. While this scheme can ensure efficient shielding of the LHC aperture from transverse

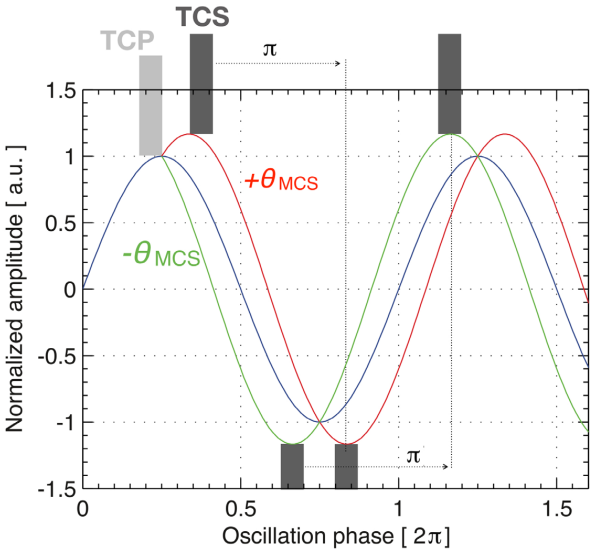

Fig. 13: Qualitative definition of optimum locations for secondary collimators in a two-stage system, in which TCSs must intercept beam particles out-scattered at the primary collimators. In this one-dimensional model, two phase locations exist, where the amplitudes caused by multiple Coulomb scattering are a maximum for the two signs of the scattering angle, $\pm\theta_{\mathrm{MCS}}$.

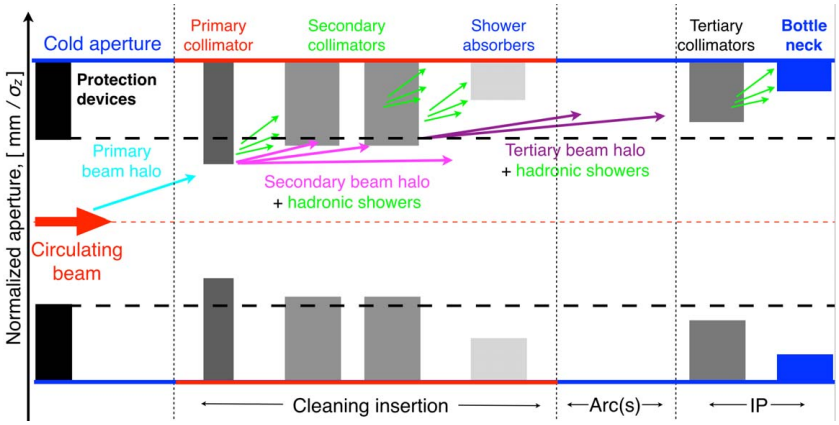

Fig. 14: Key elements of the LHC multistage collimation system: IP, interaction point

halo losses, it is not sufficient to absorb products of hadronic showers before they reach cold magnets downstream of the cleaning insert. Moreover, a two-stage system localized in a single insertion is not adequate for the local protection of critical bottlenecks that might be exposed to losses, notably the triplet magnets around the experiments that become critical during the squeeze. The collimation system of the LHC has therefore evolved into a *multistage collimation system* that includes, in addition to TCPs and TCSs, tertiary collimators (target collimators, tertiary; TCTs) in front of critical bottlenecks, shower absorbers in the warm cleaning inserts, and protection devices in the dump region, to shield the machine in case of dump kicker failures. The LHC multistage collimation system is shown in Fig. 14.

The cleaning performance of the final LHC collimation system [14] is shown in Fig. 15. While the system is described in detail in the next section, the simulations are shown here for a direct comparison with the single-stage system. The insertion regions (IRs) where the largest losses occur are the betatron (IR7) and momentum (IR3) cleaning, ATLAS (IR1) and CMS (IR5). This simulation is for beam 1 (B1), nominally 7 TeV, in collision conditions. An enlargement of the loss map around the betatron cleaning

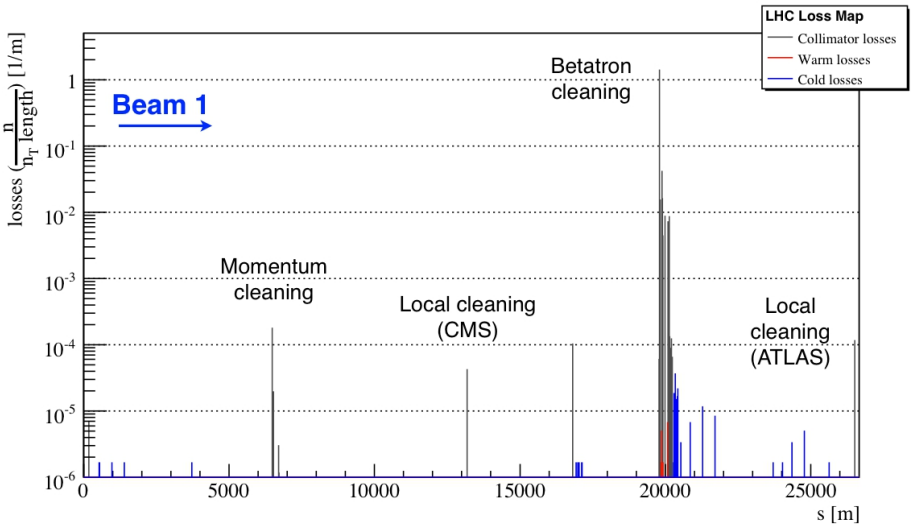

Fig. 15: Local cleaning inefficiency as a function of s for the final collimation system of the LHC run I. Loss distributions are simulated for the LHC beam 1 at 7 TeV for a perfect machine, with the collision optics squeeze to $\beta^* = 0.55$ m in IR1 and IR5. Courtesy of D. Mirarchi.

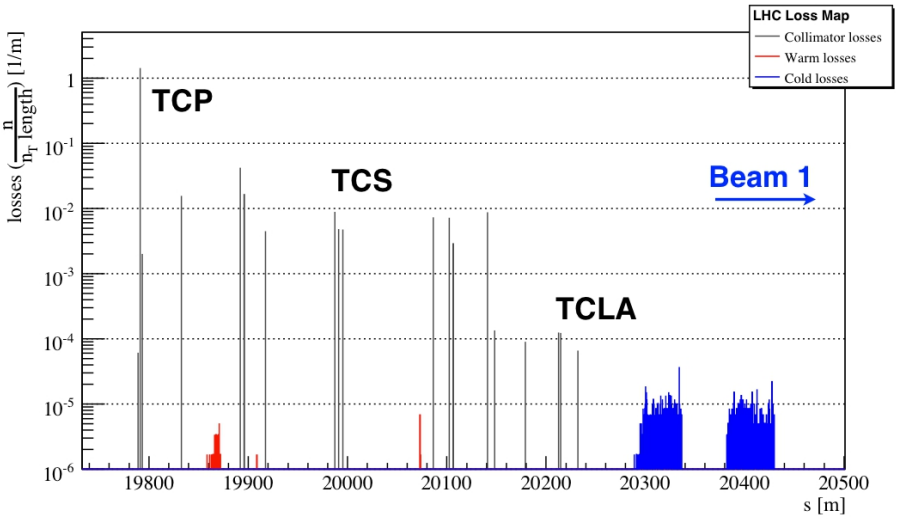

Fig. 16: Enlargement of the IR7 region of the cleaning inefficiency plot of Fig. 15. Labels indicate the approximate locations of the three families of collimator in IR7. TCLA, target collimator long absorber; TCP, target collimator (primary); TCS, target collimator (secondary).

insert is shown in Fig. 16. For a perfect machine, cold losses are now below $\sim 10^{-5}$. The highest peaks are localized in the dispersion suppressor regions downstream of IR7.

5 The LHC collimation system

The LHC collimation system was designed to handle proton beams of a stored energy of 362 MJ and is now being upgraded to cope with the design HL-LHC goal of about 700 MJ per beam. A complex and distributed system is needed to achieve the excellent halo cleaning required to operate the LHC below quench limits. In this section, the collimation layout is presented and the collimator design is reviewed. Operational challenges for the collimation at the LHC are then introduced, presenting the solutions produced to set the system up for optimum performance in all operational phases.

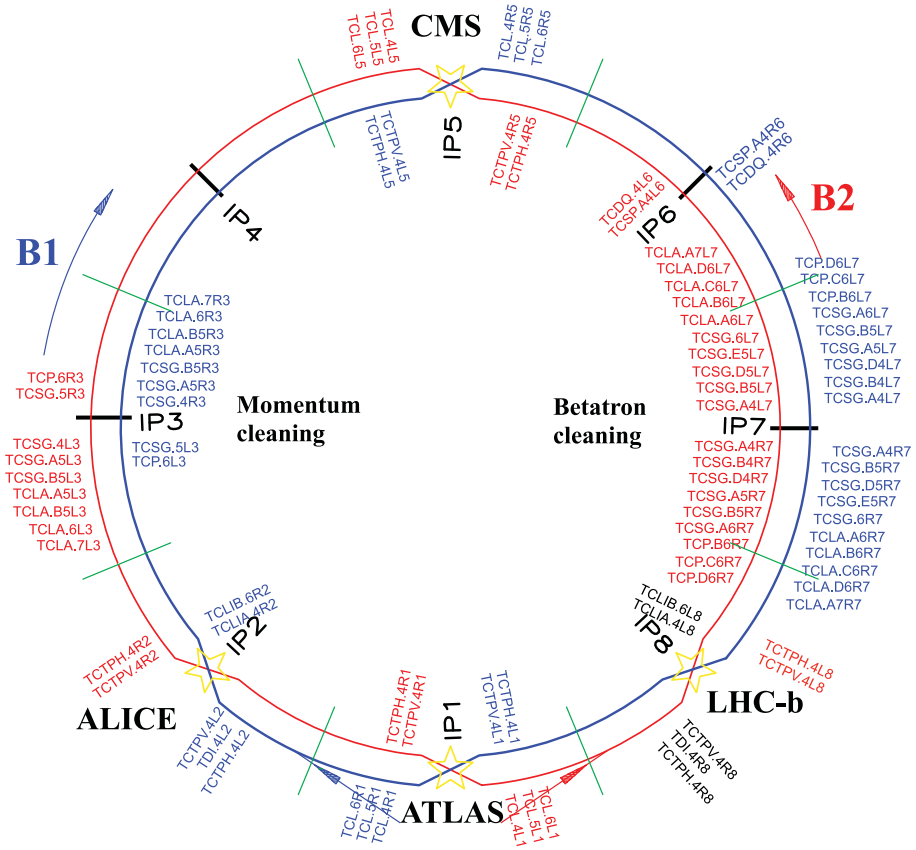

Fig. 17: Layout of the LHC, showing the collimator locations around the ring

5.1 LHC ring collimation layout

Figure 17 shows the LHC layout and the positions of the collimators around the ring. A list of collimator types, with a description of their functionality (primary, secondary, etc.) and key collimator properties is given in Table 2. Including the dump protection block (target collimator dump quadrupole, TCDQ) and the injection protection collimator (target dump, injector TDI), the system deployed for the 2015 LHC operation comprises 110 movable collimators installed in the LHC ring and its transfer lines.

Halo collimation is achieved by the multistage cleaning system introduced in Section 4. This comprises three stages in IR3 (momentum cleaning) and IR7 (betatron cleaning), where the primary collimators (TCPs), closest to the beam, are followed by secondary collimators (TCSs) and active absorbers (TCLAs). For optimal performance, the particles in the beam halo should first hit a TCP, and the TCSs should only intercept secondary halo particles that have been already scattered by, and escaped from, upstream collimators. The TCPs and TCSs, which are the closest collimators to the beam and hence intercept large beam losses, are made of a carbon fibre composite (CFC) to ensure high robustness. These collimators are also more likely to be hit by the beam if there is a failure. The TCLAs catch tertiary halo particles scattered out of the TCSs, as well as showers from upstream collimators. The TCLAs are made of a tungsten alloy, in order to stop as much as possible of the incoming energy. However, they are not as robust as the CFC collimators and should therefore never intercept primary beam losses. The setting hierarchy is chosen to ensure that this condition is respected in all operation state.

In addition to the dedicated inserts in IR7 and IR3, there are collimators in most other IRs. A pair of tertiary collimators (target collimators, tertiary, pick-up; TCTPs), made of a tungsten alloy, are installed in both beams about 150 m upstream of the collision points for all experiments, one TCTP in the horizontal plane (TCTPH) and one in the vertical (TCTPV). They provide local protection of the quadrupole triplets in the final focusing system, which are the limiting cold apertures during physics

Table 2: List of movable LHC collimators for run II. CFC, carbon fibre composite; H, horizontal; S, skew; V, vertical.

Functional type	Name	Plane	Number	Material
Primary IR3	TCP	H	2	CFC
Secondary IR3	TCSG	H	8	CFC
Absorbers IR3	TCLA	H,V	8	W alloy
Primary IR7	TCP	H,V,S	6	CFC
Secondary IR7	TCSG	H,V,S	22	CFC
Absorbers IR7	TCLA	H,V	10	W alloy
Tertiary IR1/2/5/8	TCTP	H,V	16	W
Physics debris absorber	TCL	H	12	Cu/W alloy
Dump protection	TCSP	H	2	CFC
	TCDQ	H	2	C
Injection protection (lines)	TCDI	H,V	13	CFC
Injection protection (ring)	TDI	V	2	C
	TCLI	V	4	CFC
	TCDD	V	1	CFC

operation. They are also important for decreasing the experimental background. Downstream of the high-luminosity experiments, ATLAS and CMS, there are three TCLs (target collimator, long) per beam, to intercept the collision debris. Furthermore, at the beam extraction in IR6, dump protection collimators are installed as a protection against miskicked beams in the case of extraction failures. Similarly, there are injection protection collimators in IR2 and IR8.

During the long LHC shutdown in 2013 and 2014, 18 new collimators based on a beam position monitor design [27], in which beam position monitor pick-ups are embedded in the jaws to measure the beam position at the collimator location, have been installed. They replaced the TCSGs (target collimator, secondary, graphite) in IR6 and the tertiary collimators in all experiments, as these locations are considered more critical for orbit control, in order to enhance LHC performance [28]. These collimators are called TCTP and TCSP, where 'P' stands for pick-up.

5.2 Optics and layout of cleaning inserts

The optics and layout of the betatron and momentum cleaning inserts are shown in Figs. 18 and 19, respectively. In both inserts, four *dog-leg* dipoles, called D4 and D3, are placed symmetrically on either side of the 'IP7', and are used to enlarge the beam–beam separation from 194 mm to 224 mm, making more transverse space for collimators. The two D4 magnets also delimit the $\approx$500 m long warm insert, which comprises the warm quadrupoles Q4 and Q5. The Q6 quadrupoles on either side of the D4 dipoles are the first superconducting magnets before the beam enters the cold arc.

In IR7, three primary collimators intercept horizontal, vertical, and skew halos. They are located in the region between the D3 and D4 dipoles, i.e., on the upstream side of the warm insertion for each beam. This maximizes the length of the warm section downstream of the primary loss location. A similar implementation is adopted in IR3, where, however, only one horizontal TCP is needed, placed at a location with large normalized dispersion, $D_x/\sqrt{\beta_x}$, to intercept particles with energy deviations. Momentum cleaning in one plane is sufficient, as at the LHC, vertical dispersion is negligible. The IR3 primary collimator needs to be at larger transverse betatron amplitudes than those of the IR7, to decouple the functionalities of the two inserts. Typical transverse betatron amplitudes expressed in units of σ_x as

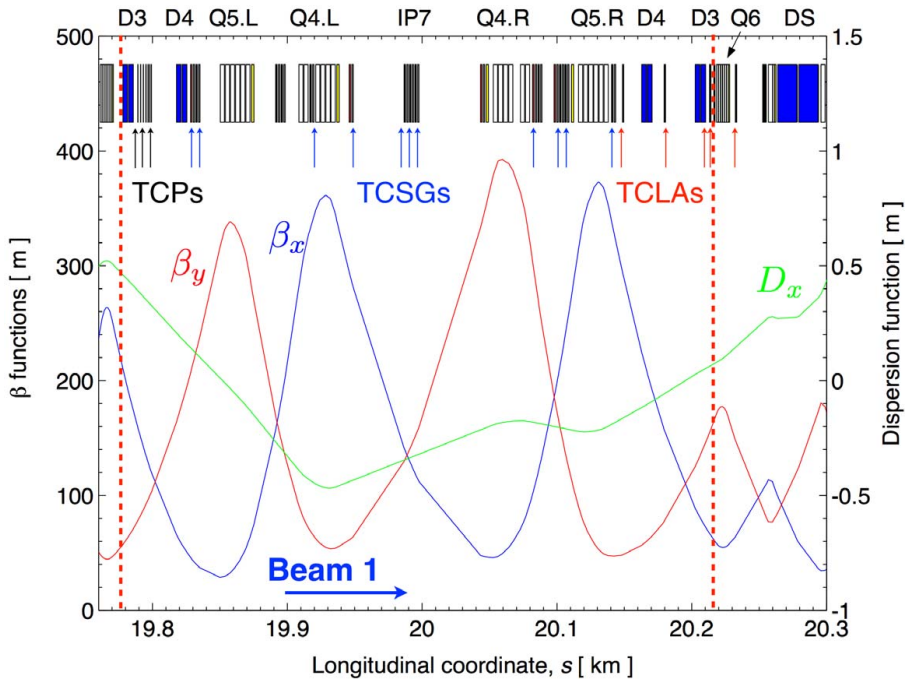

Fig. 18: Betatron (β_x, β_y) and dispersion (D_x) functions as a function of s in the LHC betatron cleaning insertion IR7. The main layout elements are also shown: quadrupoles (white boxes), dipoles (blue), and collimators (black). Vertical arrows indicate the installed collimators: 3 TCPs, 11 TCSGs; 5 TCLAs. Vertical red dashed lines indicate the limits of the warm regions (Q6 magnets at either side of IP7 are the first cold magnets). D, dipole magnet; IP, interaction point; L, left; R, right; Q, quadrupole magnet; TCLA, target collimator long absorber; TCP, target collimator (primary); TCSG, target collimator (secondary, graphite).

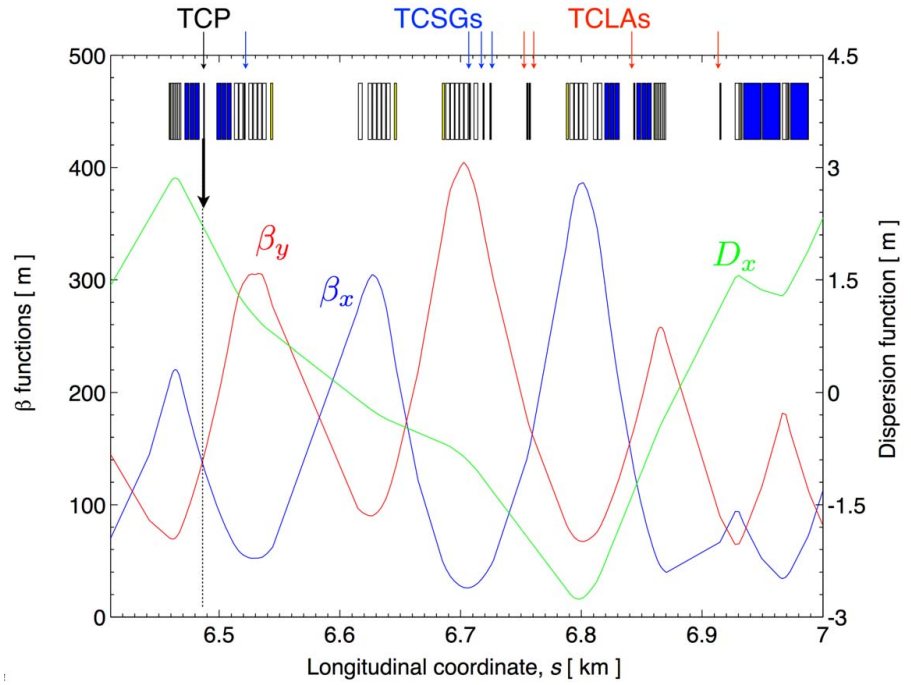

Fig. 19: Betatron (β_x, β_y) and dispersion (D_x) functions as a function of s for B1 in the LHC momentum cleaning insertion IR3. Vertical arrows indicate the installed collimators: 1 TCP, 4 TCSGs; 4 TCLAs. The main layout elements are also shown: quadrupoles (white boxes), dipoles (blue), and collimators (black). TCLA, target collimator long absorber; TCP, target collimator (primary); TCSG, target collimator (secondary, graphite).

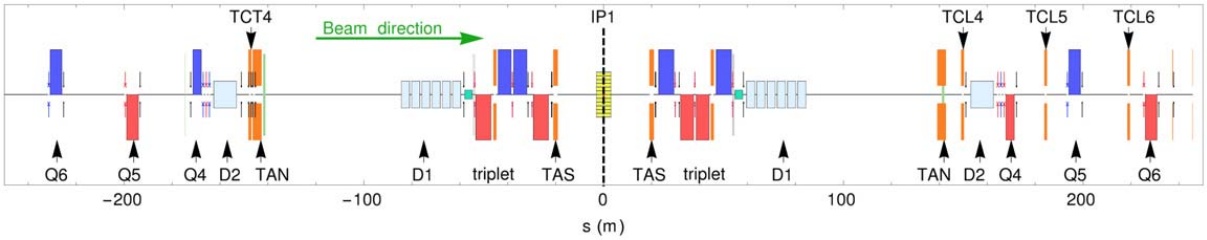

Fig. 20: Layout elements around IR1 (ATLAS) in the 2015 configuration of the LHC collimation system. D, dipole; IP, insertion point; Q, quadrupole; TAN, target absorber (neutral); TAS, target absorber (secondary); TCL, target collimator (long); TCT, target collimator (tertiary). Courtesy of R. Bruce.

in Eq. (3) are 2.5–3 times larger than in IR7, to ensure that IR3 does not act as a betatron system for particles with small energy errors.

The collimators of IR3 and IR7 are indicated in Figs. 18 and 19 by black boxes. Eleven TCS collimators are used in IR7, whereas four are used in IR3, since collimation occurs in one plane only. Five active absorbers (TCLAs) are used in IR7 and four in IR3. These devices, of types TCP, TCSG, and TCLA (see Table 2) are all two-sided collimators. Even if a one-sided collimator might be sufficient for a multiturn cleaning process, two-sided collimators are crucial for precise alignment of the circulating beams.

The layout of IR1 (ATLAS) is shown in Fig. 20. A pair of horizontal and vertical TCTPs protect the triplet from incoming beam losses. Three TCL-type physics debris absorbers protect the magnets downstream of the IR from collision products. The other high-luminosity experiment, CMS in IR5, has an equivalent layout. For IR2 (ALICE) and IR8 (LHCb), there is no need for a TCL collimator because the lower luminosity values do not put the matching sections at risk of quenching.

In addition to the movable collimators, 10 passive absorbers are also mounted in front of the most exposed warm magnets of each collimation insert: the D3 magnets downstream of the TCPs and the first modules of the Q5 and Q4 quadrupoles. These fixed-aperture collimators, called TCAPs, dramatically reduce the radiation doses to magnet coils, increasing their lifetimes by a factor of 10 or more (chapter 18 of [1]).

5.3 Operational challenges and beam-based set-up

5.3.1 LHC operational cycle and recap. of machine configurations

The main phases of the LHC operational cycle, which is periodically run to prepare for periods of physics data acquisition ('stable beam' mode), are injection, energy ramp, betatron squeeze, and preparation of collisions ('adjust' mode). The squeeze, in which the optics around the interaction points are changed to reduce the colliding beam sizes, has so far been performed at constant flat-top energy. In this phase, the betatron function is enlarged at the inner triplets as required to reduce the β^* values, i.e., the beta functions at the collision points.

The LHC design value of β^* for the high-luminosity points IP1 (ATLAS) and IP5 (CMS) is 55 cm for a beam energy of 7 TeV, limited by the available triplet aperture. During LHC run I, a β^* value of 60 cm was achieved at 4 TeV. The first year, 2015, of LHC run II started with a β^* value of 80 cm at 6.5 TeV, to ease recommissioning after the 2 year shutdown [29] but it is planned to move to a β^* value close to 40 cm in 2016. These excellent results were achieved thanks to a better aperture than had been anticipated during the LHC design phases, which was also better than the one used to specify various LHC systems. For the scope of this lecture, it is still useful to review the system design by starting from the design values.

5.3.2 *Collimation settings strategy in the LHC operational cycle*

The LHC aperture was reviewed in Section 3; see Table 1. With an injection stored energy of 22 MJ, i.e., not only above the quench limit but also significantly above the damage limit of metals [18], beam collimation is required in every phase of the LHC operational cycle, from injection to collision. Particularly challenging are the dynamic phases (energy ramp, betatron squeeze, and change of orbit configurations), when collimator movements must be synchronized precisely with other accelerator systems, such as power converters and RF units. This operation mode imposes tight constrains on the collimator control design.

At the injection, distributed aperture bottlenecks are expected in the arcs, as the magnet aperture was designed to fit the beams at injection [1]. At 7 TeV, the arc aperture is no longer critical because the betatron amplitudes are damped at larger beam energies. The aperture is now limited by the triplets, where β functions of up to $\approx$4500 m are required to achieve small beam sizes at the interaction points. By design (see Table 1), the normalized apertures, $\hat{A}_{\mathrm{min},z}$, are actually similar for the two extreme cases. Thus, even if the accelerator physics motivations are different, similar collimator settings are deployed at injection and in physics conditions. This involves moving collimators to follow the shrinking beam envelope.

Figure 21 shows an example of collimator settings at injection (top) and 3.5 TeV (bottom), taken from the operation configuration of the LHC 2010 run [30]. The horizontal beam envelope at $5.7\sigma_x$, as defined by the TCP gaps, is shown, together with the values of the collimator half gap projected on the horizontal plane at each collimator (magenta bars). The TCPs were kept at a normalized aperture of $5.7\sigma_z$ at all energies. The TCSGs were moved from $6.7\sigma_z$ to $8.5\sigma_z$, and the TCLAs were moved from $10.0\sigma_z$ to $17.7\sigma_z$. These relaxed top-energy settings were conceived to reduce the operational tolerances in the first year of the run [30] and were then subsequently tightened to improve the cleaning performance [31], reaching $4.3\sigma_z$ in 2012. The collimator gap values in millimetres, as used for the 4 TeV operation at $\beta^* = 60$ cm are shown in Fig. 22, where the transverse clearance left by the IR7 primary collimators and the distribution of gaps are shown. The smallest gap is 2.1 mm.

It is clear from Fig. 21 that a basic requirement for the LHC collimator design is that the jaws must be movable, as the gaps required at top energy to ensure optimum performance are not compatible with the larger beam sizes at injection. The need for small gaps at top energy also has important effects on the operational strategy of the collimation system because it necessitates dedicated beam-based alignment procedures, as collimators cannot be set deterministically to such small gaps without direct measurements to 'find' the local beam position and size.

5.3.3 *Beam-based set-up of LHC collimators*

he LHC collimation system performance relies on respecting the well-defined hierarchy between collimator families. In practice, this involves knowing the beam orbit and beam size at each collimator, as shown in Fig. 23. With beam sizes as small as 200 μm and orbit offsets of up to 2–3 mm, and in the presence of collimator alignment errors of up to a few hundred micrometres, the determination of optimum jaw positions can only be achieved through a series of measurements aimed at measuring the required parameters, which are referred to as *beam-based collimator alignments*.

The procedure for collimation set-up at the LHC (Fig. 24) was established [30,32] based on experience gained with a prototype LHC collimator installed for beam tests in the Super Proton Synchrotron (SPS) [33]. The beam halo is shaped with a reference collimator (1), typically a primary collimator, which is closed to a known half gap of $3 - 5\sigma$. This reference halo is used to cross-align other collimators, by moving their jaws towards the beam in small steps of 5–20 μm until the halo is *touched*, with symmetrical beam loss responses from either jaw (2). This gives the local orbit position. The reference collimator is then closed further (3) until it touches the halo again: this enables the gaps of the two collimators to be cross-calibrated. The average of the initial and final gaps of the reference collimator in

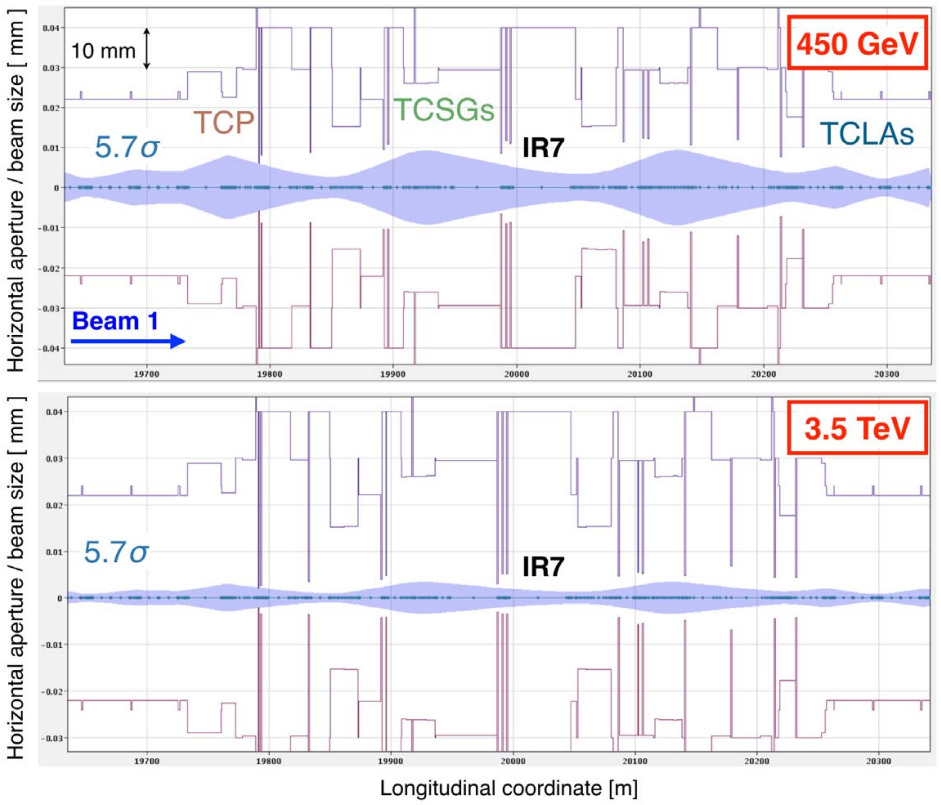

Fig. 21: Horizontal aperture, collimator jaw positions (vertical bars) and 5.7σ beam envelope at (top) injection and (bottom) 3.5 TeV in betatron cleaning (IR7) from the LHC on-line model application [30]. IR, insertion region; TCG, target collimator (graphite); TCLA, target collimator (long absorber); TCP, target collimator (primary).

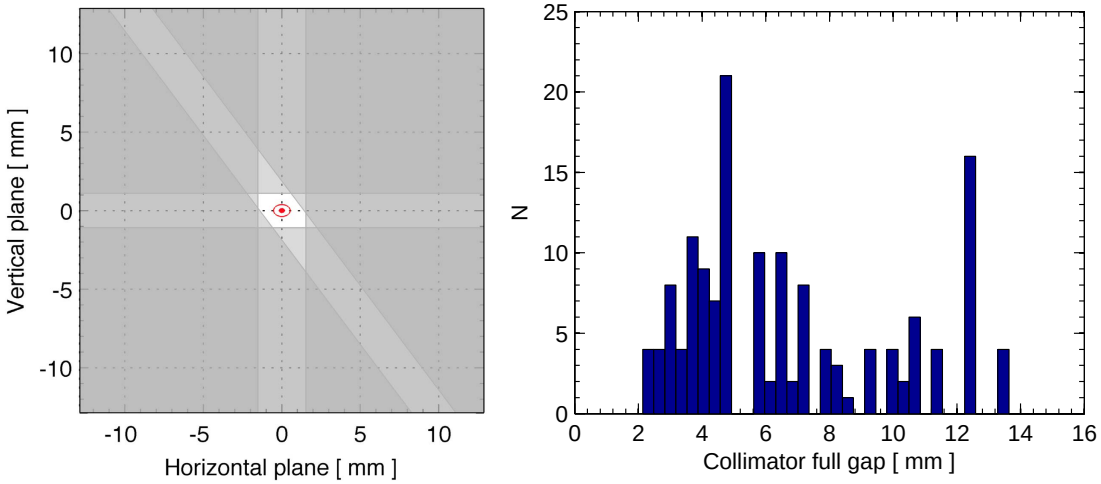

Fig. 22: Left: Beam clearance for the LHC beams, as defined by the primary collimator gaps. Right: Distribution of collimator gaps, as adopted for operation at 4 TeV and $\beta^\star = 60$ cm in 2012. In 2015, the same IR7 settings in millimetres are used for the 6.5 TeV operation.

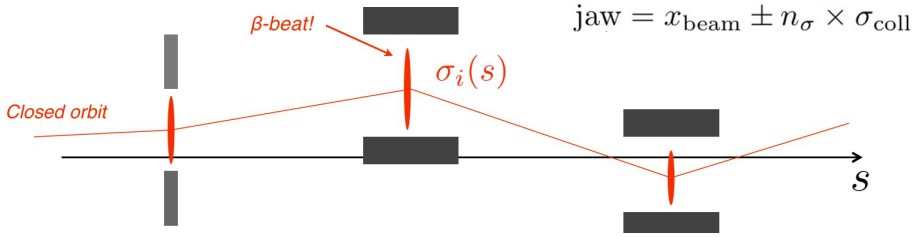

Fig. 23: Collimator jaw positions at various locations in the ring, where the closed orbit and beam size are different. Proper collimator set-up requires direct measurements of beam position and size, to ensure that the collimator hierarchy is respected.

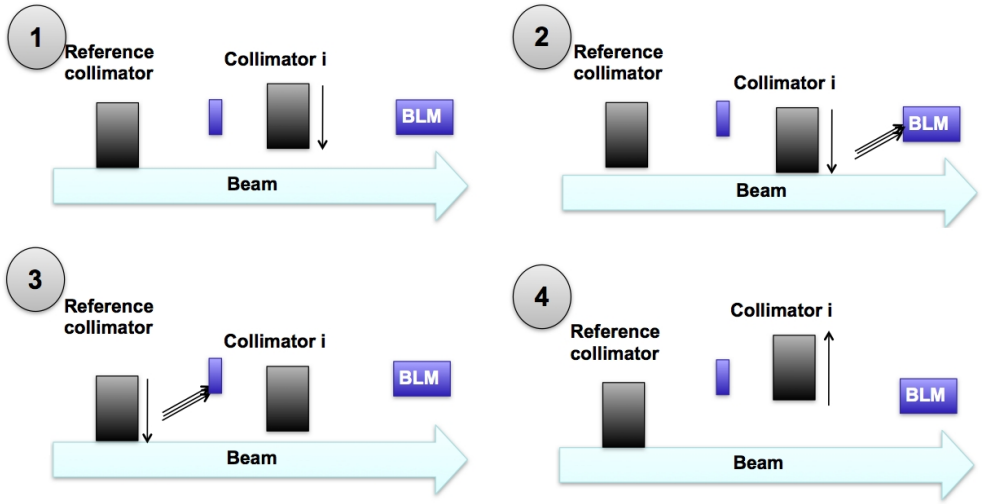

Fig. 24: The collimator set-up procedure used to determine beam orbit and relative beam size to that of a reference collimator, for operational settings generation [32]. BLM, beam loss monitor.

units of n_σ gives the normalized gap of the other collimator. Finally, the latter collimator is opened to its nominal settings (4). This ensures that the relative retraction with respect to the reference collimator is respected, even in the presence of different beta-beating at the two locations. An example of *beam-based collimator centres* measured in 2012 is shown in Fig. 25. This reinforces the previous assertion that beam-based alignment is mandatory for a proper collimator set-up at the LHC.

This set-up procedure is precise but time consuming. During the initial commissioning in 2010, it was carried out manually for each collimator. An automated feedback system between collimator movements and the beam loss monitor signal has been developed, enabling the set-up time to be improved significantly and dramatically reducing the number of spurious beam aborts from human error. A detailed treatment of this optimization of beam-based alignment is beyond the scope of this lecture but can be found in Ref. [34].

5.3.4 Collimator setting generation for operation

Beam-based alignment must be done for each collimator in the ring, for every relevant machine configuration (injection, top energy before and after squeeze, collision). To minimize the risk of damaging the collimators while approaching them to the beams, the alignment is carried out with the minimum intensity that allows reliable orbit measurements, i.e., with a few bunches of nominal bunch intensity. Let us now assume that the local orbit, x_{beam}, and beam size, σ_{coll}, are calculated at every collimator in each discrete point of the operational cycle.

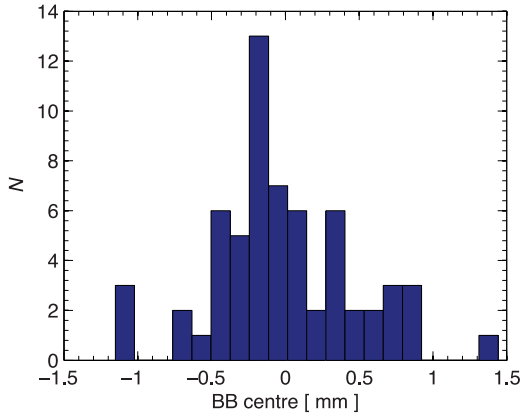

Fig. 25: Distribution of beam-based centres of LHC collimators as a result of the alignment campaign of 2012. Shifts of up to more than 1.5 mm are found from the cumulative effects of orbit misalignments, electronics offsets of the beam position monitor system, alignment error of the collimators with respect to the reference orbit, etc.

While collimators are installed in a variety of azimuthal orientations (see Fig. 26), the jaw movement is in one dimension, along the collimator plane. For arbitrary collimator angles θ_{coll}, the *effective* beam size in the collimation plane, σ_{coll} is computed from the horizontal and vertical sizes as

$$\sigma_{\text{coll}} = \sqrt{\sigma_x^2 \cos(\theta_{\text{coll}})^2 + \sigma_y^2 \sin(\theta_{\text{coll}})^2} \,, \tag{14}$$

where σ_z, $z \equiv (x, y)$, is calculated as in Eq. (3). The collimator half gap is calculated as $h = n_\sigma \times \sigma_{\text{coll}}$ and the jaw positions around the beam position, x_{beam}, are given by

$$\text{jaw} = x_{\text{beam}} \pm n_\sigma \times \sigma_{\text{coll}} \,. \tag{15}$$

Note that each jaw has two motors, which allow the tilt angle to be adjusted with respect to the beam envelope. In the following, the tilt angle is assumed to be zero. Stepping motors can be driven through arbitrary functions of time. The motion of collimators around the ring can be synchronized through timing events at the microsecond level [35, 36]. This is necessary to ensure optimum collimator settings during critical machine phases, such as the energy ramp and the betatron squeeze. To this end, continuous setting functions must be generated from the beam-based parameters through scaling rules versus beam energy and optics.

Let us calculate, for example, the ramp functions, starting from settings values at injection ('0') and flat-top ('1'). The half gap during the energy ramp is expressed as a function of the energy:

$$h(\gamma) = n_\sigma(\gamma) \times \sigma_{\text{coll}}(\gamma) \,, \tag{16}$$

where $\gamma = \gamma(t)$ is the relativistic gamma function. For the LHC, it is sufficient to use linear functions in γ for n_σ and σ_{coll}. A linear interpolation between the beam-based parameters at injection and flat-top yields:

$$h(\gamma) = \left[n_{\sigma,0} + \frac{n_{\sigma,1} - n_{\sigma,0}}{\gamma_1 - \gamma_0}(\gamma - \gamma_0) \right] \times \frac{1}{\sqrt{\gamma}} \left[\frac{\sqrt{\epsilon_1 \beta_1} - \sqrt{\epsilon_0 \beta_0}}{\gamma_1 - \gamma_0}(\gamma - \gamma_0) \right] \,. \tag{17}$$

The beam centre is also expressed as a linear function of γ to give the jaw position as

$$\text{jaw}(\gamma) = \left[x_{\text{beam},0} + \frac{x_{\text{beam},1} - x_{\text{beam},0}}{\gamma_1 - \gamma_0}(\gamma - \gamma_0) \right] \pm h(\gamma) \,. \tag{18}$$

Note that the beam size $\sigma_{\text{coll}} = \sigma_{\text{coll}}(\gamma)$ is also a function of the optics and therefore might change, typically for the tertiary collimators in the experimental regions, during the betatron squeeze [37]. This

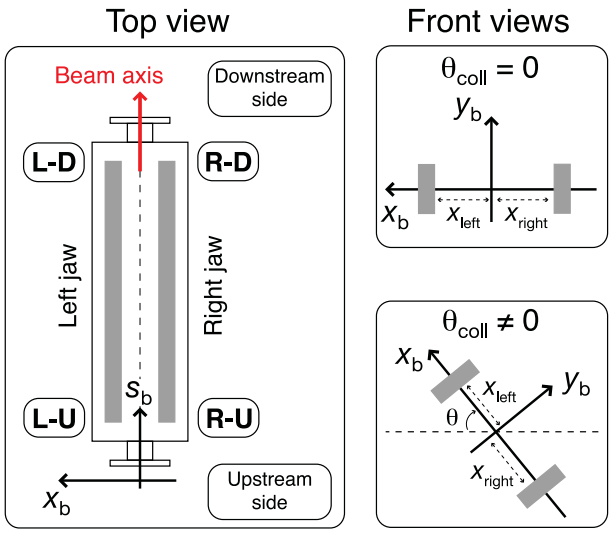

Fig. 26: Top and front views of a collimator, with labels and naming conventions. Each jaw has two motors that move the jaws in the collimation plane: horizontal ($\theta_{\text{coll}} = 0$), vertical ($\theta_{\text{coll}} = \pi/2$) or skew planes. D, downstream; L, left; R, right; U, upstream.

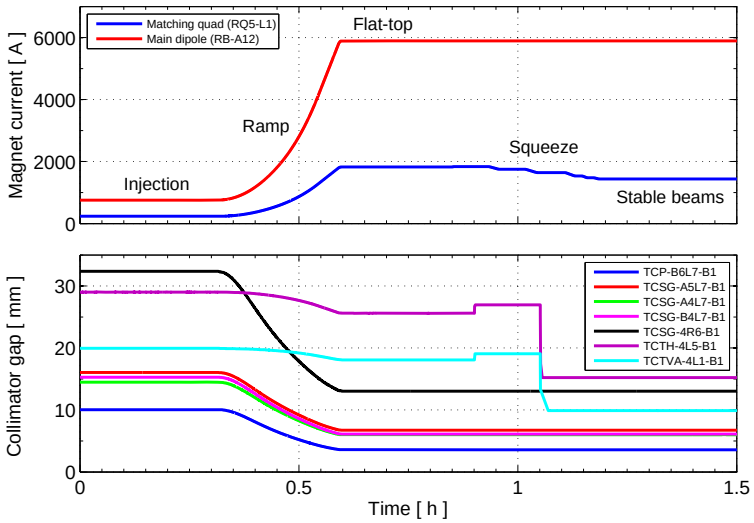

Fig. 27: Operational cycle for selected collimators for a typical LHC fill. Top: Measured magnet currents versus time. Bottom: Collimator gaps versus time.

notation can be generalized in a straightforward way by considering functions of β^* instead of γ for the parameters involved. An example of collimator gaps versus time during a full LHC cycle is given in Fig. 27 (bottom graph), together with the LHC dipole and matching quadrupole currents, to indicate the times of the ramp and squeeze phases (top graph).

The operation of the collimation system is automated by sequences that are run at every fill, enabling operation crews to run smoothly through the different sets of the cycle settings. The operation mode can only work thanks to the excellent stability of the LHC orbit and optics and of the collimator hardware itself. So far, only one beam-based alignment per year has been required [38].

Table 3: Minimal horizontal and vertical apertures at injection (450 GeV) for warm and cold elements

Parameter	Value
High stored beam energy	360 MJ/beam
Large transverse energy density	1 GJ/mm^2
Activation of collimation inserts	1–15 mSv/h
Small spot sizes at high energy	≈200 μm
Collimation close to beam	6–7σ
Small collimator gaps	2.1 mm (at 7 TeV)
Big and distributed system	110 devices, ≈500 degrees of freedom

6 Collimator design for high-power accelerators

The key parameters for the design of the LHC collimator are summarized in Table 3. The list emphasizes the challenges in terms of quenching of superconducting magnets, damage, heating of components and radiation doses, which must be addressed by a optimized design. It is important to note that the design must ensure adequate mechanical stability during jaw position changes and in the presence of important heat loads. Other aspects related to materials choice to ensure robustness and limited impedance are addressed in a companion paper [18]. Details of the final collimator design deployed for the LHC can be found in Refs. [14, 39]. Here, only the main design features are given.

The LHC collimators are high-precision devices that ensure the correct hierarchy along the 27 km long ring with beam sizes as small as 200 μm. Each collimator has two jaws, of different lengths and materials, depending on functionality (Table 2). Each jaw can be independently moved by two stepping motors. Key features of the design are: (1) a jaw flatness of about 40 μm along the 1 m long active jaw surface; (2) a surface roughness less than 2 μm; (3) a 5 μm positioning resolution; (4) an overall setting reproducibility below 20 μm [35]; (5) a minimal gap of 0.5 mm; (6) evacuated heat loads of up to 7 kW in a steady-state regime and of up to 30 kW in transient conditions.

Primary and secondary collimators are made of a robust CFC that is designed to withstand beam impacts without significant permanent damage for the worst failure cases, such as impacts of a full injection batch of $288 \times 1.15 \times 10^{11}$ protons at 450 GeV and of up to $8 \times 1.15 \times 10^{11}$ protons at 7 TeV [39]. Other collimators made of heavy tungsten alloy or copper, obviously, do not have the same robustness and are only utilized at larger distances from the circulating beams, where maximum absorption is needed.

The cross-section of the primary and secondary collimator jaws, with a 2.5 cm thick active CFC part and a cooling system underneath, is shown in Fig. 28. The design drawing on the right side of the picture is compared with a real jaw prototype on the left, built during the initial production phases to verify the manufacturing quality. Two parallel jaws are mounted in the vacuum tank, as shown in Fig. 29 for a primary collimator. In Fig. 29, the jaws are actually shown set to the operational position for the vertical collimator with the tightest gaps, as in Fig. 22.

Figure 30 shows a horizontal and a 45° tilted LHC collimator. Their vacuum tank is still open to show the CFC jaws inside. An example of the tunnel installation layout for a IR7 collimator is given in Fig. 31. This is a horizontal TCLA collimator. Notice, next to the collimator, a yellow support that supports a vacuum pump that is installed next to each collimator. A beam loss monitor, not visible in the photograph, is also connected to this support, to record losses generated locally when the beam is intercepted by the collimator jaws.

The collimator design has been recently improved by adding two beam position monitors on either extremity of each jaw [27]. An example of a CFC jaw prototype with this new design is shown in Fig. 32. This feature allows faster collimator alignment as well as constant monitoring of the beam orbit at the

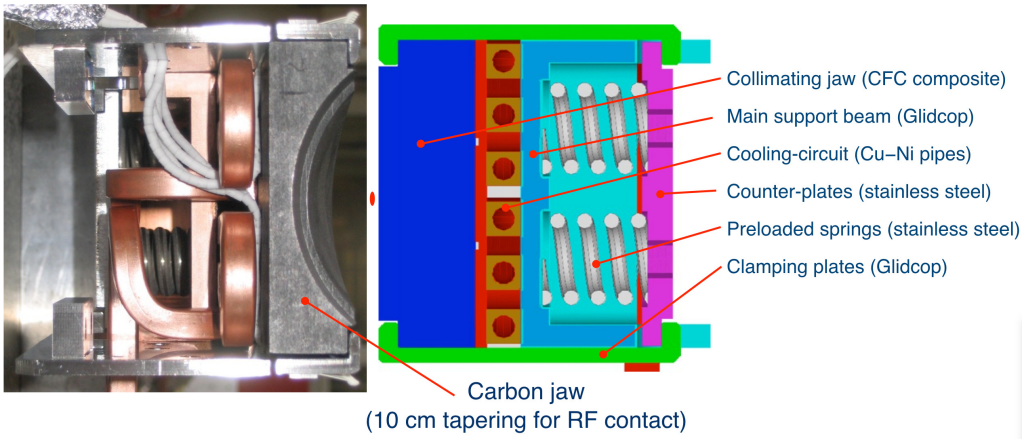

Fig. 28: Cross-section of the LHC collimator jaws. Left: real prototype. Right: design drawing. The position of the beam is shown by the red ellipse, as if the two jaws were those of a horizontal collimator. A sandwich structure, with cooling circuits clamped on the CFC plate of the active part, is optimized to minimize deformation of the structure during steady loss conditions [39].

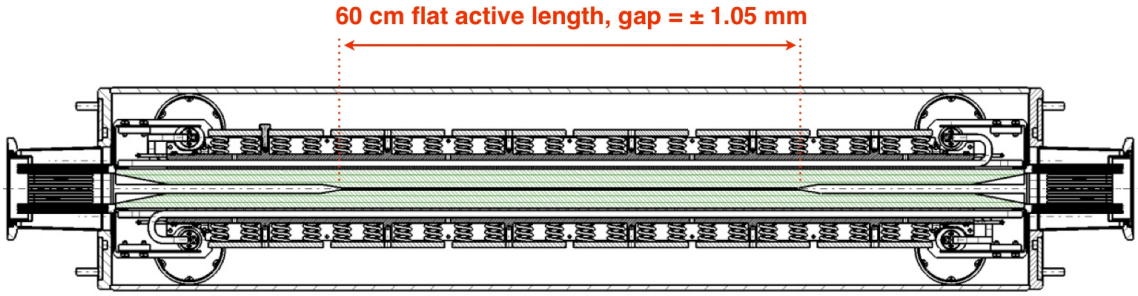

Fig. 29: Design of the LHC primary collimator. The two jaws can move independently, thanks to four stepping motors enabling position and angular adjustment with respect to the beam. This design is essentially identical to that of the secondary collimator except that the jaws are tapered to an effective length of 60 cm instead of 100 cm.

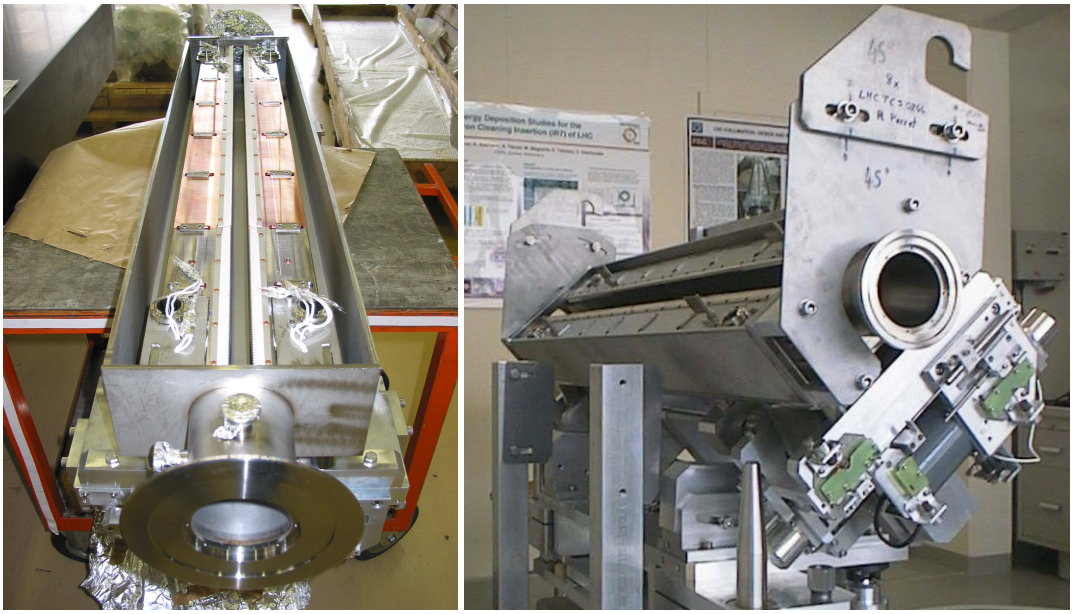

Fig. 30: Horizontal (left) and skew (right) LHC collimators with open tank, showing movable jaws. The support allows assembly in the same collimator tank of all the required orientations.

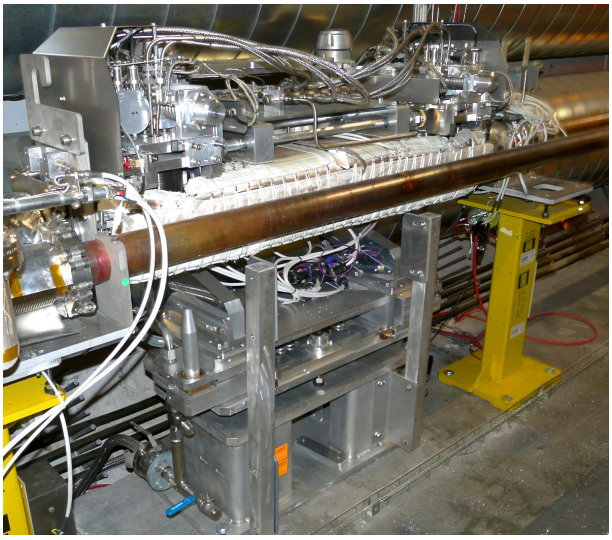

Fig. 31: Active absorber TCLA.B6R7.B1 as installed in the betatron cleaning insert. The stepping motors that control jaw position and angle are visible on top of the vacuum tank. The pipe of the opposing beam is also shown.

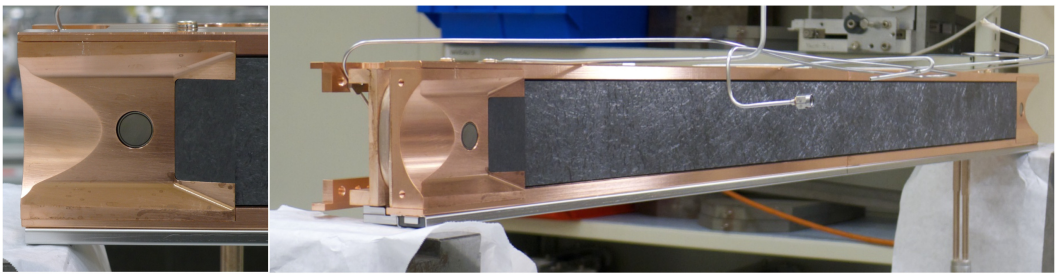

Fig. 32: New CFC jaw with integrated beam position monitors at each extremity for installation in IR6 (see Fig. 17). A variant of this design, made with a Glidcop support and tungsten heavy alloy inserts on the active jaw part, is used for the new TCTP tertiary collimators in all IRs.

collimator, as opposed to the beam-loss-monitor-based alignment that can currently only be performed during dedicated low-intensity commissioning fills. The beam position monitor buttons will improve collimation performance significantly in terms of operational efficiency and flexibility, by reducing the machine time spent on aligning collimators and the β^* reach [39]. The beam-position-monitor-embedded design is considered the baseline for future upgraded collimator design.

7 Cleaning performance of the LHC beam collimation

The cleaning performance of the LHC collimation system is measured by intentionally generating transverse and off-momentum beam losses while measuring losses around the ring. This is done with low intensities circulating in the machine. A few bunches are excited by driving the betatron tune close to resonance or by adding transverse noise with the transverse damper. The latter method is preferred, as it can act in a bunch-by-bunch mode so one fill can be used for several loss maps. Large losses of the momentum cleaning can instead be generated by changing the radio frequency. These so-called *loss maps* are used to validate, empirically, the response of the collimation system in the presence of high loss rates. This is an essential part of the validation of the LHC machine protection functionality, as discussed in Ref. [9]. In particular, loss maps are used to verify: (1) that the hierarchy is respected, by checking that the relative loss rates at the different collimators are in agreement with predictions or within tolerable levels; (2) that the leakage of losses to the other machine equipment, in particular

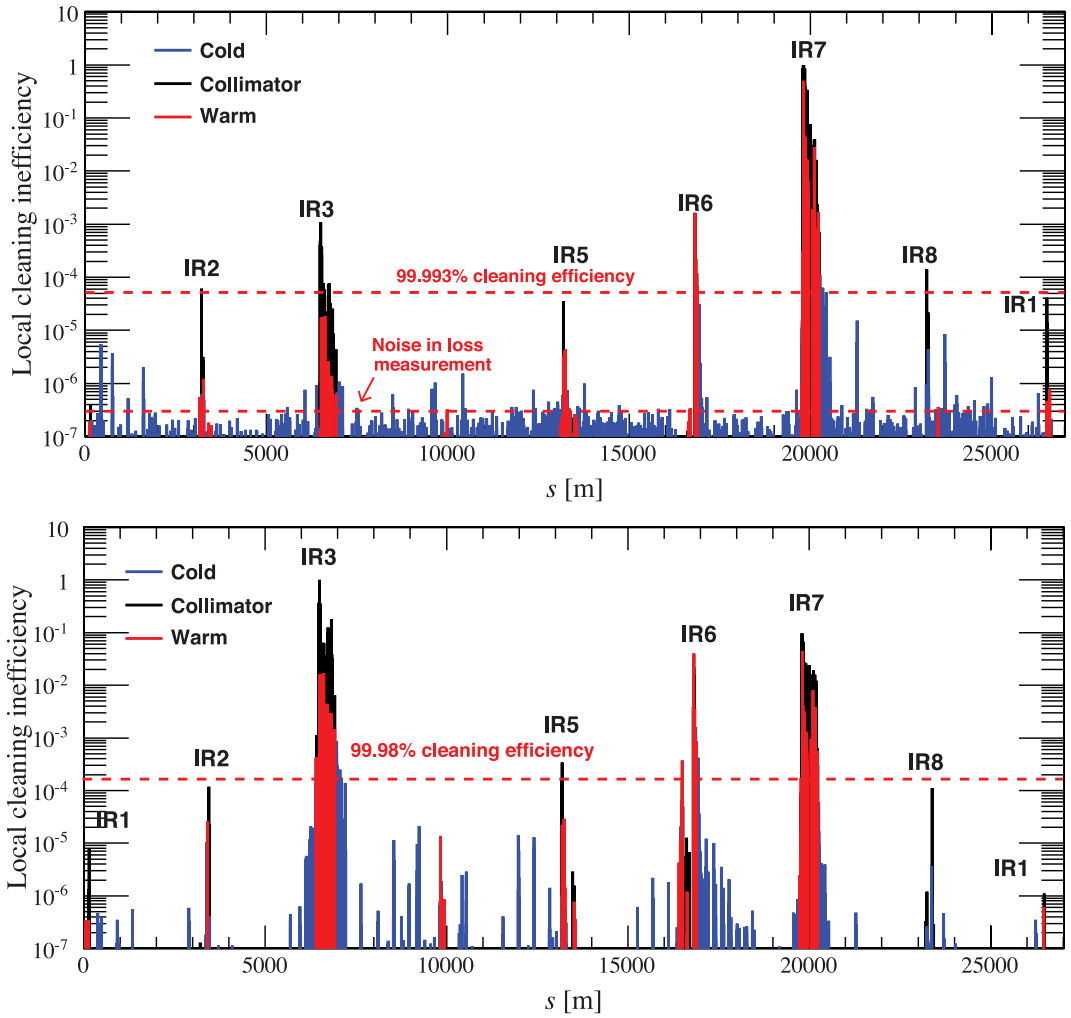

Fig. 33: Betatron (top) and off-momentum (bottom) loss maps obtained at the LHC at 4 TeV with beams squeezed to 60 cm in IR1 (ATLAS) and IR5 (CMS), showing the beam losses recorded at about 4000 beam loss monitors around the ring, normalized to the highest measured signal. Betatron losses are generated in IR7 by adding noise to the kickers of the transverse damper of clockwise beam 1. IR3 losses are generated by changing the radio frequency until the full beam is intercepted by the IR3 TCP. Both beams are excited at the same time as their frequencies are synchronized. Courtesy of B. Salvachua [38].

superconducting magnets, are as expected; (3) that the system performance remain stable during long periods when beam-based alignment is not repeated.

Examples of betatron and off-momentum loss maps are shown in Fig. 33. These maps were recorded in 2012 at 4 TeV, with beams squeezed to 60 cm in IR1 and IR5. At the LHC, beam losses are recorded by about 3600 beam loss monitors around the ring [40]. To estimate the cleaning inefficiency, losses at each monitor are normalized to the highest measured signal, i.e., next to the primary collimators. This is shown in Fig. 33 as a function of the longitudinal coordinate s. It is seen that inefficiencies less than $\sim 10^{-4}$ were achieved. In all IRs, the largest losses are recorded at the collimators (black bars), as expected. The cold locations with the highest losses are the dispersion suppressors downstream of the cleaning insert, as predicted in simulations (see Fig. 15).

The IR7 losses are given in Fig. 34. The limiting locations with the worst cleaning are the dispersion suppressors on either side of IR7 (the right side for beam 1). A cleaning efficiency above 99.993% was achieved. Note that, with the exception of a few isolated peaks in the dispersion suppressor, the

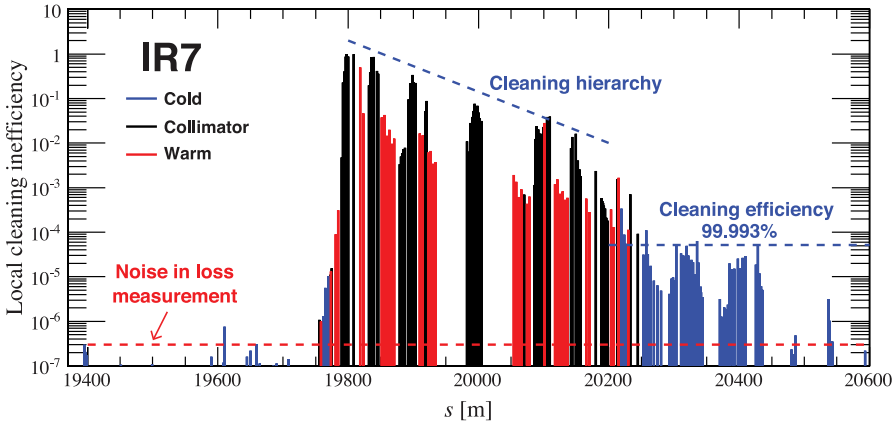

Fig. 34: Enlargement of the top graph of Fig. 33, showing details of losses in IR7. The limiting location for betatron cleaning is given by the losses on the cold magnets in the dispersion suppressor immediately downstream of IR7.

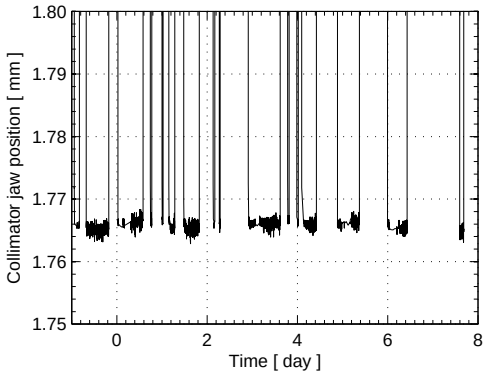

Fig. 35: End-of-ramp settings for one TCP jaw as a function of time over 9 days, showing micrometre reproducibility [30].

rest of the cold machine experiences losses that are more than one order of magnitude smaller, i.e., close to the noise of the beam loss monitor system. In simulations, losses are sampled using 10 cm bins, counting the number of beam particles hitting the aperture. In measurements, losses are measured at the discrete locations of beam loss monitors that record the flux of ionizing particles in the beam loss monitor volume. Clearly, these two quantities cannot be directly compared without additional simulations of energy deposition, starting from the multiturn loss pattern. Detailed discussion of this aspect is beyond the scope of this lecture. It suffices to say that the agreement between simulations and measurements is good [41].

The fill-to-fill reproducibility of the collimator positions is of the order of a few micrometres. A typical example for one jaw of a TCP collimator is given in Fig. 35. This is a key ingredient for the system performance because the collimator settings are not realigned. This stability of the hardware, together with the outstanding fill-to-fill reproducibility of optics and orbit at the LHC, makes it possible to maintain excellent collimation performance with one single beam-based alignment per year in IR3/6/7. As an example, in Fig. 36 the cleaning inefficiencies at the worst locations in the rings are shown for each beam and loss plane. It can be seen that the stability of the measured cleaning is indeed remarkable.

8 Advanced collimation concepts for enhanced beam collimation

Other advanced collimation concepts have been under study in the last year, as possible methods of improving the performance of the LHC multistage system. In this section, the main topics presently under

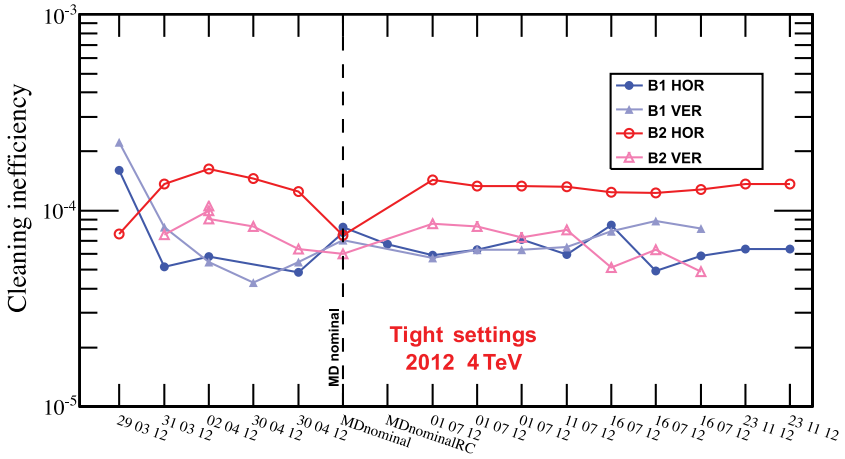

Fig. 36: Collimation cleaning inefficiency at the worst location in the dispersion suppressors at either side of IR7 for both beams and planes, as measured throughout the 2012 operation with protons (4 TeV, $\beta^* = 60$ cm). B, beam; HOR, horizontal; VER, vertical. Courtesy of B. Salvachua [38].

investigation are introduced. Possible immediate applications of such advanced concepts are already under consideration for the high-luminosity upgrade of the LHC.

8.1 Local dispersion suppressor cleaning

Protons and ions interacting with the collimators in IR7 emerge from the IR with a changed magnetic rigidity. This represents a source of local heat deposition in the cold dispersion suppressor magnets downstream of IR7, where the dispersion starts to increase: these losses are the limiting locations for collimation cleaning, i.e., they are the highest cold losses around the ring. This may pose a certain risk for inducing magnet quenches, in particular, in view of the higher intensities expected for HL-LHC. This problem arises for halo collimation of both proton and heavy-ion beams.

A possible solution to this problem is to add local collimators in the dispersion suppressors, which is only feasible with a major change of the cold layout at the locations where the dispersion starts to increase. Indeed, the existing system's multistage cleaning is not efficient at catching these dispersive losses. Clearly, the need for local collimation depends on the absolute level of losses achieved in operation and the quench limit of superconducting magnets. In view of the uncertainties in the scaling of the current system performance for operation at 7 TeV, it is important to take appropriate margins, to minimize the risk of limitation in the future.

A solution with minimum impact on the cold section layout is to replace the existing 15 m long dipoles with two shorter, higher-field magnets, by freeing enough space to install a warm collimator. This solution is illustrated in Fig. 37. It requires an 11 T dipole field to free sufficient space for a warm collimator to be installed in a dedicated cryogenics by-pass system, as shown in Fig. 38. Even in this tight space limitation, an adequate solution can be found. New dipoles and collimators are being prototyped at CERN, providing a viable solution for IR7 cleaning upgrades that might already be available for a long LHC stop planned for 2019. Note that this solution is modular and was designed to be implemented easily in any existing dipole location. It can therefore also be used to improve cleaning around collision points, if necessary, as is foreseen for the ALICE ion experiment [42].

8.2 Status on research and development on novel collimator materials

The LHC impedance budget is largely dominated by the contribution of the LHC collimators. For this reason, the current collimation system was conceived in such a way that it can be easily upgraded to reduce the impedance [14]: every secondary collimator slot in IR3 and IR7 features a companion slot

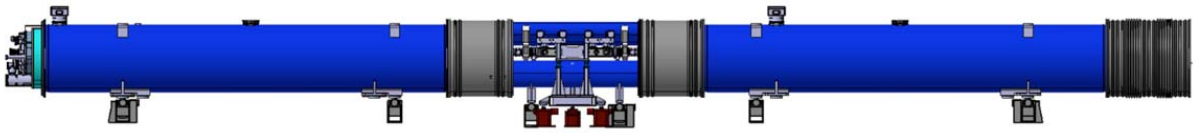

Fig. 37: Longitudinal integration of a TCLD collimator between two short 11 T dipoles. Courtesy of D. Ramos

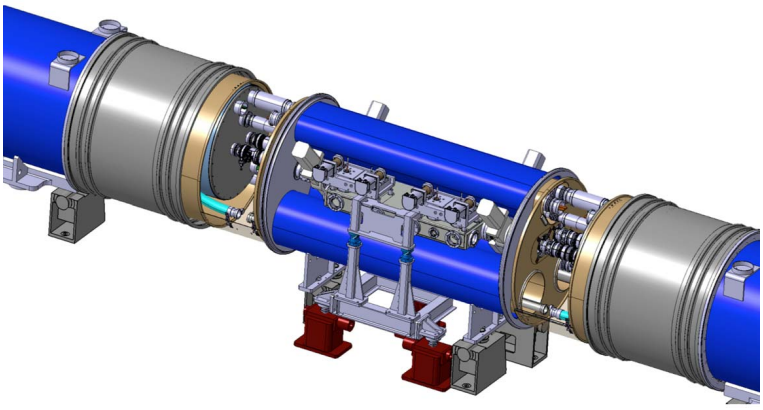

Fig. 38: Three-dimensional view of the TCLD installation in the cryogenic by-pass region between two 11 T dipoles. Courtesy of D. Ramos and L Gentini.

for the future installation of a low-impedance secondary collimator. A total of 22 slots in IR7 and 8 slots in IR3 are already cabled for a quick installation of new collimators—referred to as TCSPMs—which can either replace or supplement the existing TCSG collimators. The TCSPMs will include pick-ups for orbit measurements ('P') and will be based on metal composites ('M'). In addition, limited robustness against beam losses of the present tungsten collimator has already limited the LHC performance of run I in terms of β^* reach, because adequate margins had to be taken in the collimation hierarchy to shield the existing tertiary collimators properly [28].

A rich programme of research and development was initiated, to find novel material with optimum response to thermomechanical stress and with reduced impedance, to improve various limitations of current LHC collimator materials. More details are given in a companion paper [18]. Simulations predict that beam stability can be re-established for all HL-LHC scenarios if the CFC of the existing secondary collimators is replaced, at least in the betatron cleaning insertion (IR7), with a jaw material having an electrical conductivity a factor of 50 to 100 higher than CFC [43]. This improvement could easily be achieved if the jaw material were made of highly conductive metals, such as copper or molybdenum. However, secondary collimators in IR7 also play a crucial role in LHC machine protection and might be exposed to large beam losses. Therefore, collimator materials and designs must also be robust against beam failure. The driving requirements for the development of new materials are thus: (i) low resistive-wall impedance, to avoid beam instabilities; (ii) high cleaning efficiency; (iii) high geometrical stability, to maintain the precision of the collimator jaw during operation despite temperature changes; and (iv) high structural robustness, in case of accidental events, such as single-turn losses.

The current baseline for the upgraded secondary collimators relies on novel carbon-based materials, such as molybdenum carbide-graphite (MoGr), a ceramic composite jointly developed by CERN and Brevetti Bizz, in which the presence of carbides and carbon fibres strongly catalyses the graphitic ordering of carbon during high-temperature processing, enhancing its thermal and electrical properties (Fig. 39). To further improve their surface electrical conductivity, these materials could be coated with pure molybdenum or other lower-Z refractory coatings. Replacing all existing CFC secondary collimators in both IR7 and IR3 with bulk MoGr or MoGr coated with 5 µm thick pure molybdenum would reduce the total LHC impedance by 40% or 60%, respectively.

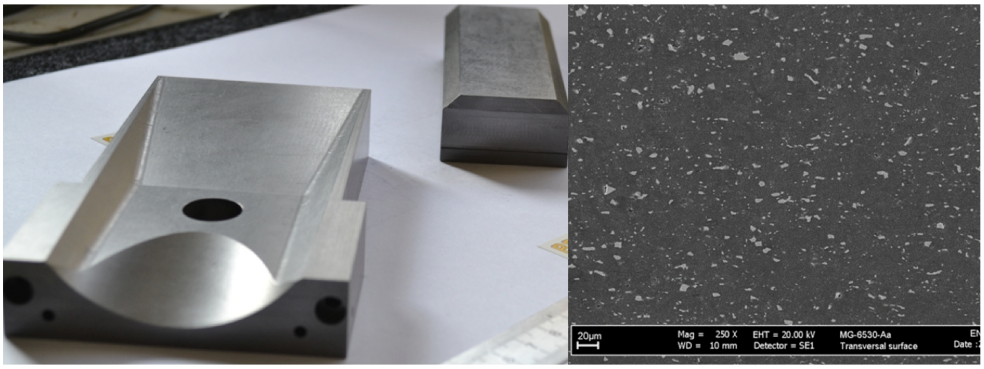

Fig. 39: Left: MoGr components recently produced by Brevetti Bizz (Italy) for a jaw prototype. Jaw extremity (dimensions of $147 \times 88 \times 25$ mm^3) and jaw absorbing block ($125 \times 45x \times$ mm^3) are shown. A jaw assembly includes two jaw extremities (taperings) and eight blocks. Right: Detail of microstructure; the graphite matrix is visible, together with molybdenum carbide grains of about 5 µm. Courtesy of A. Bertarelli.

The new collimator design, along with novel materials and possible alternative coatings must be validated for operation in the LHC. For these purposes, a rich programme of validation is in progress, involving tests at the CERN HiRadMat facility [44], to address robustness against beam impact, mechanical engineering prototyping, beam tests at the LHC, and experimental verification of the material response under high radiation doses. It is anticipated that this test will be completed, and the production of new, low-impedance, highly robust collimators in the LHC started, by 2019.

8.3 Halo diffusion control techniques

The 2012 operation experience indicates that the LHC collimation would profit from halo control mechanisms. The idea is that, by controlling the diffusion speed of halo particles in an aperture range between the core and the TCP opening ($\approx$3–5σ_z), one can act on the time profile of the losses. The main goal is to reduce loss rates that would otherwise take place in a short time, or simply to control the static population of halo particles in a certain aperture range. For example, it is expected that losses caused by orbit drifts [45] during the squeeze (see Figs. 5 and 6) can be strongly reduced by actively depleting the halo population.

One of the best candidate techniques for achieving active halo control at the LHC is to use the hollow e-lens collimation concept [46, 47]. A hollow electron beam, running coaxially to the proton or ion beam, is used to generate an annular beam in the transverse (x, y) plane. This hollow beam induces an electromagnetic field, which affects halo particles above a certain transverse amplitude and can change their transverse speed. The working principle is illustrated in Fig. 40. A solid experimental basis achieved at the Tevatron indicates that this solution is very promising for the LHC. The design for an hollow e-lens for the LHC is ongoing (see [48] and references therein).

Conversely, in the case of loss spike limitations at the LHC during run II, the hollow e-lens solution would not be viable because it could only be implemented over a time-scale of a few years [49]. It is, therefore, crucial to work on alternatives that, if necessary, might be implemented on an appropriate time-scale. Two alternatives are currently being considered: tune modulation through noise in the current of lattice quadrupoles, as outlined in Ref. [50], and narrow-band excitation of halo particles, using the transverse damper system. Though very different from the hardware point of view, both these techniques rely on exciting tail particles through resonances induced in the tune space. This method works on the assumption that there is a correlation between halo particles with large amplitudes and corresponding tune shifts in tune space (de-tuning with amplitude). Clearly, both methods require solid experimental verification in a very low noise machine, like the LHC, in particular, to demonstrate that these types of excitation do not perturb the beam core emittance. Unlike hollow e-lenses, which act directly in the transverse plane by affecting particles at amplitudes above the inner radius of the hollow beam, resonance

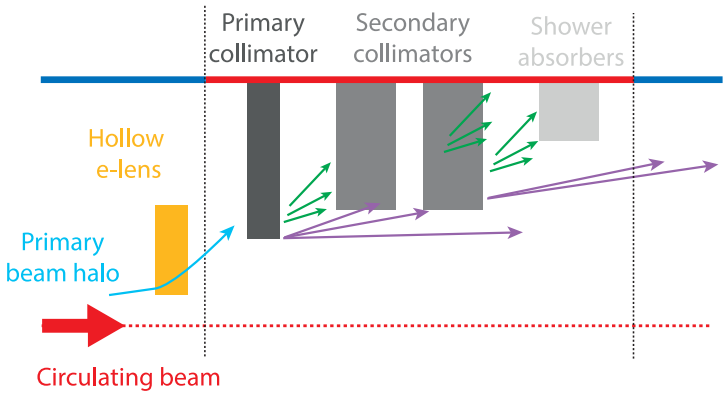

Fig. 40: Integration of hollow e-lenses as halo diffusers in the present collimation system.

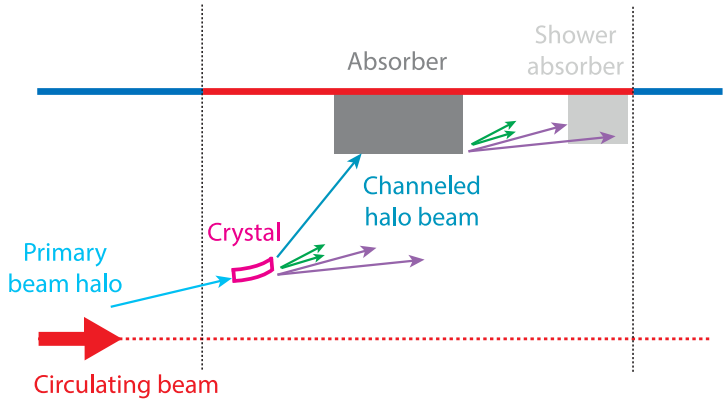

Fig. 41: Crystal collimation concept foreseen the use of a bent crystal to channel halo particle in one single passage to a dedicated absorber, reducing significantly the number of secondary collimators.

excitation methods require a good knowledge of the beam core and tail particle tunes, even in dynamic phases of the operational cycle. It is planned to test these techniques experimentally in LHC run II.

8.4 Crystal collimation

Highly pure bent crystals can be used to steer high-energy particles that become trapped between the potential of parallel lattice planes [51]. Equivalent bending fields of up to hundreds of teslas can be achieved in crystals with a length of only 3–4 mm, enabling, in principle, halo particles to be steered to a well-defined point, with obvious potential applications to beam collimation. As opposed to standard primary collimators based on amorphous materials, which require several secondary collimators and absorbers to catch the products developed through the interaction with matter (Fig. 14), one single absorber per collimation plane is, in theory, sufficient in a crystal-based collimation system. This is shown in Fig. 41.

In addition to the reduction of secondary collimators, nuclear interactions with well-aligned crystals are much reduced compared with a primary collimator, provided that high channelling efficiencies of halo particles can be achieved (particles impinging on the crystal are to be channelled within a few turns). This is expected to reduce dispersive beam losses in the dispersion suppressor of the betatron cleaning insertion significantly, compared with the existing system, which is limited by the leakage of particles from the primary collimators. Simulations indicate a possible gain of between 5 and 10 [52], even for a layout without an optimized absorber design. The crystal collimation option is particularly interesting for collimation of heavy-ion beams, thanks to the reduced probability of ion dissociation and fragmentation compared with current primary collimators.

Another potential of crystal collimation is a strong reduction of the machine impedance, since (1) only a small number of collimator absorbers is required and (2) the absorbers can be spaced much farther apart, owing to the large bending angle from the crystal (40–50 μrad instead of a few microradians from multiple Coulomb scattering in the primary collimator). Conversely, an appropriate absorber design must be conceived to handle the design peak loss rates, of 1 MW during 10 s, expected for the LHC upgrade [2]. Other potential issues concern the machine protection aspects of this scheme, which has not yet been studied in detail, and operational aspects for crystals that require mechanical angular stability in the submicroradian range through the operational cycle. Note that the critical angle beyond which channelling is lost is ≈2 μrad at 7 TeV.

Promising results were achieved in dedicated crystal collimation tests at the SPS, performed from 2009 within the UA9 experiment [53–55]. However, some outstanding issues on the feasibility of the crystal collimation concept for the LHC can only be addressed by beam tests at high energy in the LHC. For this purpose, a study at the LHC has been proposed, and will take place in the LHC run II [52, 56]. Tests at the LHC will address the feasibility of the crystal collimation concept with LHC beam conditions, in particular, to demonstrate that such a system can provide better cleaning than the present high-performance system throughout the operational cycle.

Acknowledgements

The material presented here is the result of the work of many people and was presented on behalf of the LHC collimation project team. Past and present team members are gratefully acknowledged. In particular, R. Bruce, D. Mirarchi, B. Salvachua, and G. Valentino are sincerely thanked, for providing material for this document and for providing useful comments on the manuscript.

References

[1] LHC design report, Vol. 1. The LHC main ring, edited by O.S. Brüning *et al.*, CERN-2004-003-V-1 (CERN, Geneva, 2004), http://dx.doi.org/10.5170/CERN-2004-003-V-1

[2] L. Rossi, LHC upgrade plans: options and strategy, Proc. 2nd Int. Particle Accelerator Conf., San Sebastian, 2011 [*Conf. Proc. C* **110904** (2011) 908].

[3] L. Rossi *et al.*, HL-LHC preliminary design report, CERN-ACC-2014-0300 (2014). `https://cds.cern.ch/record/1972604/files/CERN-ACC-2014-0300.pdf`

[4] N. Mokhov *et al.*, *J. Instrum.* **6** (2011) T08005. http://dx.doi.org/10.1088/1748-0221/6/08/T08005

[5] H. Hahn *et al.*, *Nucl. Instrum. Methods Phys. Res.* A **499**(2–3) (2003) 245. http://dx.doi.org/10.1016/S0168-9002(02)01938-1

[6] M. Lamont, The first years of LHC operation for luminosity production, Proc. 4th Int. Particle Accelerator Conf. (IPAC 2013), 12–17 May 2013, Shanghai, China. C13-05-12 (2013) p. MOYAB101.

[7] B. Auchmann *et al.*, *Phys. Rev. ST Accel. Beams* **18**(6) (2015) 061002. http://dx.doi.org/10.1103/PhysRevSTAB.18.061002

[8] R. Schmidt, Introduction to accelerator protection course, these proceedings.

[9] J. Wenninger, Machine protection and operation for LHC, these proceedings.

[10] R. Bruce *et al.*, *Nucl. Instrum. Methods Phys. Res.* A **729** (2013) 825. http://dx.doi.org/10.1016/j.nima.2013.08.058

[11] G. Valentino *et al.*, *Phys. Rev. ST Accel. Beams* **16**(2) (2013) 021003. http://dx.doi.org/10.1103/PhysRevSTAB.16.021003

[12] K.H. Mess and M. Seidel, *Nucl. Instrum. Methods Phys. Res.* A **351**(2-3) (1994) 279. http://dx.doi.org/10.1016/0168-9002(94)91354-4

[13] H. Burkhardt *et al.*, Collimation down to 2 sigmas in special physics runs in the LHC, Proc. 4th Int. Particle Accelerator Conf. (IPAC 2013), 12–17 May 2013, Shanghai, China. C13-05-12, CERN-ACC-2013-0144 (2013).

[14] R. Aßmann *et al.*, The final collimation system for the LHC, Proc. 10th European Particle Accelerator Conf., Edinburgh, UK, 26–30 June 2006, CERN-LHC-Project-Report-919 (2006), p. 986.

[15] R. Aßmann, Collimators and cleaning: could this limit the LHC performance? LHC Performance Workshop, Chamonix XII, Chamonix, France, 2003.

[16] S. Redaelli *et al.*, LHC aperture and commissioning of the collimation system, Proc. Chamonix 2005 LHC Project Workshop, Chamonix, France, 2005, CERN-AB-2005-014 (2005), p. 268.

[17] V. Kain, Beam dynamics and beam losses—circular machines, these proceedings.

[18] A. Bertarelli, Beam-induced damage mechanisms and their calculation, these proceedings.

[19] G. Robert-Demolaize *et al.*, A new version of SixTrack with collimation and aperture interface [*Conf. Proc. C* **0505161** (2005) 4084].

[20] F. Cerutti, Beam material interaction, heating and activation, these proceedings.

[21] S. Redaelli, M. C. Alabau-Pons, M. Giovannozzi, G. Muller, F. Schmidt, R. Tomas and J. Wenninger, "LHC Aperture Measurements," Conf. Proc. C **100523**, MOPEC010 (2010).

[22] R.W. Aßmann *et al.*, "Aperture Determination in the LHC Based on an Emittance Blowup Technique with Collimator Position Scan," Conf. Proc. C **110904**, 1810 (2011).

[23] J.B. Jeanneret and R. Ostojic, Geometrical acceptance in LHC ver. 5.0, CERN-LHC-PROJECT-NOTE-111 (1997).

[24] S. Redaelli *et al.*, Aperture and optics—measurements and conclusions, Proc. 3rd Evian Workshop on LHC beam operation, Evian-les-bains, France, 12–14 Dec 2011, CERN-ATS-2012-083 (2012), p. 77.

[25] M. Seidel, The proton collimation system of HERA, DESY-94-103 (1994).

[26] J.B. Jeanneret, *Phys. Rev. ST Accel. Beams* **1**(8) (1998) 081001. http://dx.doi.org/10.1103/PhysRevSTAB.1.081001

[27] F. Carra *et al.*, LHC collimators with embedded beam position monitors: a new advanced mechanical design, Proc. IPAC2011, San Sebastian, IPAC-2011-TUPS035 (2011).

[28] R. Bruce *et al.*, *Phys. Rev. ST Accel. Beams* **18**(6), (2015) 061001. http://dx.doi.org/10.1103/PhysRevSTAB.18.061001

[29] R. Bruce *et al.*, Baseline LHC machine parameters and configuration of the 2015 proton run, Chamonix2014: LHC Performance Workshop, Chamonix, France, 22–25 September 2014, p. 100.

[30] S. Redaelli *et al.*, Operational performance of the LHC collimation, Proc. HB2010 workshop, Morschach, CH (2010). `http://epaper.kek.jp/HB2010/`

[31] R. Bruce *et al.*, LHC β^* reach in 2012, LHC Operation Workshop, Evian, 2011. `http://indico.cern.ch/event/155520`

[32] D. Wollmann *et al.*, First cleaning with LHC collimators [*Conf. Proc. C* **100523** (2010) TUOAMH01].

[33] S. Redaelli *et al.*, Operational experience with a LHC collimator prototype in the CERN SPS, Proc. PAC09, Vancouver, Canada, 2009.

[34] G. Valentino, Ph.D. thesis, University of Malta (2103). Also as CERN-THESIS-2013-208 (2013) and CERN-ACC-2014-0062 (2014).

[35] A. Masi *et al.*, Measured performance of the LHC collimator low-level control system, Proc. ICALEPCS09, Kobe, Japan, 2009.

[36] S. Redaelli *et al.*, Final implementation and performance of the LHC collimator control system, Proc. PAC09, Vancouver, Canada, 2009.

[37] S. Redaelli *et al.*, Performance of ramp and squeeze at the Large Hadron Collider, Proc. HB2010 workshop, Morschach, CH (2010). http://epaper.kek.jp/HB2010/

[38] B. Salvachua *et al.*, Cleaning performance of the LHC collimation system up to 4 TeV, Conf. C13-05-12 (2013), p. MOPWO048.

[39] A. Bertarelli *et al.*, The mechanical design for the LHC collimators, Proc. EPAC2004, Lucerne (2004), p. 545. http://accelconf.web.cern.ch/accelconf/e04/papers/moplt008.pdf

[40] B. Dehning, Beam loss monitors at the LHC, these proceedings.

[41] R. Bruce *et al.*, *Phys. Rev. ST Accel. Beams* **17**(8) (2014) 081004. http://dx.doi.org/10.1103/PhysRevSTAB.17.081004

[42] R. Bruce *et al.*, Conceptual design of IR collimation, WP5 report of the FP7-HiLumi programme, CERN-ACC-2014-0293 (2014). https://cds.cern.ch/record/1972595/files/CERN-ACC-2014-0293.pdf

[43] E. Métral *et al.*, Intensity limitations, WP5 report of the FP7-HiLumi programme, CERN-ACC-2014-0297 (2014). https://cds.cern.ch/record/1972601/files/CERN-ACC-2014-0297.pdf

[44] H. Gaillard *et al.*, HiRadMat: a new irradiation facility for material testing at CERN [*Conf. Proc. C* **110904** (2011) 1665].

[45] S. Redaelli, *et al.*, Experience with high-intensity beam scraping and tail populations at the Large Hadron Collider, Proc. 4th Int. Particle Accelerator Conf., Shanghai, China, 12–17 May 2013, C13-05-12 (2013), p. MOPWO039, CERN Report CERN-ACC-2013-0063 (2013).

[46] V. Shiltsev, Proc. 3rd CARE-HHH-APD Workshop (LHC-LUMI-06), Valencia, Spain, CERN-2007-002 (2007), p. 92.

[47] V. Shiltsev, Proc. CARE-HHH-APDWorkshop (BEAM07), Geneva, Switzerland, CERN-2008-005 (2008), p. 46.

[48] G. Stancari *et al.*, Conceptual design of hollow electron lenses for beam halo control in the Large Hadron Collider, CERN-ACC-2014-0248 (2014).

[49] S. Redaelli *et al.*, Plans for deployment of hollow electron lenses at the LHC for enhanced beam collimation, Proc. 6th Int. Particle Accelerator Conf., Richmond, VA, USA, 3–8 May 2015.

[50] O. Brüning and F. Willeke, *Phys. Rev. Lett.* **76**(20) (1996) 3719. http://dx.doi.org/10.1103/PhysRevLett.76.3719

[51] W. Scandale, *Int. J. Mod. Phys.* A **25**(S1) (2010) 70. http://dx.doi.org/10.1142/S0217751X1004992X

[52] D. Mirarchi, Ph.D. thesis, Imperial College, London, 2015.

[53] W. Scandale *et al.*, *Phys. Lett.* B **703**(5) (2011) 547. http://dx.doi.org/10.1016/j.physletb.2011.08.023

[54] W. Scandale *et al.*, *Phys. Lett.* B **726**(1-3) (2013) 182. http://dx.doi.org/10.1016/j.physletb.2013.08.028

[55] W. Scandale *et al.*, *Phys. Lett.* B **714**(2-5) (2012) 231. http://dx.doi.org/10.1016/j.physletb.2012.07.006

[56] D. Mirarchi *et al.*, Final layout and expected cleaning for the first crystal-assisted collimation test at the LHC, Proc. 5th Int. Particle Accelerator Conf., IPAC2014, Dresden, Germany, 16–20 June 2014, C14-06-16.